REVISED MANUSCRIPT (there may still be minor changes)

Title: Pantropical tree rings show small effects of drought on stem growth

Authors: Pieter A. ZUIDEMA[1], Peter GROENENDIJK[2], Mizanur RAHMAN[3], Valerie TROUET[4,5], Abrham ABIYU[6], Rodolfo ACUÑA-SOTO[7,8], Eduardo ADENESKY-FILHO[9], Raquel ALFARO-SÁNCHEZ[10,11], Claudio Roberto ANHOLETTO JUNIOR[12], José Roberto Vieira ARAGÃO[2], Gabriel ASSIS-PEREIRA[13,14], Claudia C. ASTUDILLO-SÁNCHEZ[15], Ana Carolina BARBOSA[16], Giovanna BATTIPAGLIA[17], Hans BEECKMAN[18], Paulo Cesar BOTOSSO[19], Nils BOURLAND[18], Achim BRÄUNING[20], Roel BRIENEN[21], Matthew BROOKHOUSE[22], Supaporn BUAJAN[23], Brendan M. BUCKLEY[24], J. Julio CAMARERO[25], Artemio CARRILLO-PARRA[26], Gregório CECCANTINI[27], Librado R. CENTENO-ERGUERA[28], Julián CERANO-PAREDES[28], Wirong CHANTHORN[29], Ya-Jun CHEN[30], Bruno Barçante Ladvocat CINTRA[31,32], Eladio Heriberto CORNEJO-OVIEDO[33], Otoniel CORTÉS-CORTÉS[33], Clayane Matos COSTA[34], Camille COURALET[18], Doris Bianca CRISPÍN-DE-LA-CRUZ[2,35], Rosanne D'ARRIGO[24], Diego A. DAVID[36], Maaike DE RIDDER[18], Jorge Ignacio DEL VALLE[36], Mário DOBNER JR[37], Jean-Louis DOUCET[38], Oliver DÜNISCH[39], Brian J. ENQUIST[40,41], Karin ESEMANN-QUADROS[42,43], Gerardo ESQUIVEL-ARRIAGA[28], Ze-Xin FAN[30], Adeline FAYOLLE[44,45], Tatiele Anete Bergamo FENILLI[9], M. Eugenia FERRERO[46,35], Esther FICHTLER[47], Patrick M. FINNEGAN[48], Claudia FONTANA[13], Kainana S. FRANCISCO[49], Pei-Li FU[30], Franklin GALVÃO[50], Aster GEBREKIRSTOS[51], Jorge A. GIRALDO[52], Emanuel GLOOR[21], Milena GODOY-VEIGA[27], Daniela GRANATO-SOUZA[53], Anthony GUERRA[54], Kristof HANECA[55], Grant Logan HARLEY[56], Ingo HEINRICH[57,58], Gerhard HELLE[59], Bruna HORNINK[2,13], Wannes HUBAU[60], Janet G. INGA[35], Mahmuda ISLAM[3,61], Yu-mei JIANG[62], Mark KAIB[63], Zakia Hassan KHAMISI[4], Marcin KOPROWSKI[64,65], Eva LAYME[66], A. Joshua LEFFLER[67], Gauthier LIGOT[38], Claudio Sergio LISI[34], Neil J. LOADER[68], Francisco de Almeida LOBO[69], Giuliano Maselli LOCOSSELLI[27,70], Tomaz LONGHI-SANTOS[71], Lidio LOPEZ[46], María I. LÓPEZ-HERNÁNDEZ[33], José Luís Penetra Cerveira LOUSADA[72], Rubén D. MANZANEDO[73,74], Amanda K. MARCON[50], Justin T. MAXWELL[75], Omar N. MENDOZA-VILLA[76], Ítallo Romany Nunes MENEZES[34,77], Mulugeta MOKRIA[20,51], Valdinez Ribeiro MONTÓIA[78], Eddy MOORS[79,80], Miyer MORENO[81], Miguel Angel MUÑIZ-CASTRO[82], Cristina NABAIS[83], Anuttara NATHALANG[84], Justine NGOMA[85], Francisco de Carvalho NOGUEIRA JR.[86], Juliano Morales

OLIVEIRA[87,88], Gabriela Morais OLMEDO[89], Daigard Ricardo ORTEGA-RODRIGUEZ[13], Carmen Eugenia Rodríguez ORTÍZ[90], Mariana Alves PAGOTTO[34], Shankar PANTHI[30], Kathelyn PAREDES-VILLANUEVA[91,92], Gonzalo PÉREZ-DE-LIS[93], Laura Patricia PONCE CALDERÓN[94], Leif Armando PORTAL-CAHUANA[95,13], Darwin Alexander PUCHA-COFREP[96], Nathsuda PUMIJUMNONG[23], Paulo QUADRI[97], Jorge Andrés RAMÍREZ[98], Edilson Jimmy REQUENA-ROJAS[35], Judith REYES-FLORES[33], Adauto de Souza RIBEIRO[34], Iain ROBERTSON[68], Fidel Alejandro ROIG[46,99], José Guilherme ROQUETTE[100], Ernesto Alonso RUBIO-CAMACHO[101], Raúl SÁNCHEZ-SALGUERO[102], Ute SASS-KLAASSEN[1,103], Jochen SCHÖNGART[104], Marcelo Callegari SCIPIONI[37], Paul R. SHEPPARD[4], Lucas C.R. SILVA[105], Franziska SLOTTA[106], Leroy SORIA-DÍAZ[107], Luciana K.V.S. SOUSA[108], James H. SPEER[109], Matthew D. THERRELL[110], Ginette TICSE-OTAROLA[35,111], Mario TOMAZELLO-FILHO[13], Max C.A. TORBENSON[112], Pantana TOR-NGERN[113,114], Ramzi TOUCHAN[4], Jan VAN DEN BULCKE[60], Lorenzo VÁZQUEZ-SELEM[115], Adín H. VELÁZQUEZ-PÉREZ[116], Alejandro VENEGAS-GONZÁLEZ[117], Ricardo VILLALBA[46], Jose VILLANUEVA-DIAZ[28], Mart VLAM[103], George VOURLITIS[118], Christian WEHENKEL[26], Tommy WILS[119,120], Erika S. ZAVALETA[121], Eshetu Asfaw ZEWDU[122], Yong-Jiang ZHANG[123], Zhe-Kun ZHOU[30], Flurin BABST[124,4]

Affiliations:

[1]Forest Ecology & Forest Management Group, Wageningen University, Wageningen, The Netherlands. [2]Department of Plant Biology, Institute of Biology, P.O. Box: 6109, University of Campinas (UNICAMP), 13083-970, Campinas, SP, Brazil. [3]Department of Forestry and Environmental Science, Shahjalal University of Science and Technology, Sylhet 3114, Bangladesh. [4]Laboratory of Tree-Ring Research, University of Arizona, Tucson, AZ, USA. [5]Belgian Climate Centre, Ringlaan 3, 1090 Uccle, Belgium. [6]World Agroforestry Centre (ICRAF), C/O ILRI Campus, Gurd Shola, P.O. Box 5689, Addis Ababa, Ethiopia. [7]Department of Microbiology and Parasitology, Universidad Nacional Autónoma de Mexico, Mexico City, Mexico. [8]Colegio de Geografía, Facultad de Filosofia y Letras, Universidad Nacional Autónoma de Mexico, Mexico City, Mexico. [9]Department of Forest Engineering, Universidade Regional de Blumenau, R. São Paulo 3366, Itoupava Seca, Santa Catarina, 89030-000, Brazil. [10]Higher Technical School of Agricultural and Forestry Engineering and Biotechnology, University of Castilla-La Mancha, Albacete, Spain. [11]Department of Biology, Wilfrid Laurier University, 75 University Avenue W, Waterloo, ON, N2L 3C5, Canada. [12]Forest Management Program, Mamiraua Institute for Sustainable Development, Tefé, Brazil. [13]Department of Forest Sciences, Luiz de Queiroz College of Agriculture, University of Sao Paulo, Av. Pádua Dias 11, Piracicaba - SP, 13418-900, Brazil. [14]Instituto de Pesquisas Ambientais do Estado de São Paulo, Assis, São Paulo, Brazil. [15]Facultad de Ingeniería y Ciencias, Universidad Autónoma de Tamaulipas, 87149, Ciudad Victoria, Tamaulipas, Mexico. [16]Tree-Ring Laboratory, Forest Science Department, Federal University of Lavras, 37200-900, Lavras, MG, Brazil. [17]University of Campania "L. Vanvitelli", Department of Environmental, Biological and Pharmaceutical Sciences and Technologies, via Vivaldi 43, 81100, Caserta, Italy. [18]Wood Biology Service, Royal Museum for Central Africa, Leuvense steenweg 13, 3080 Tervuren, Belgium. [19]Brazilian Agricultural Research Corporation (Embrapa), Embrapa Forestry, Estrada da Ribeira - Km 111, 83411-000, Colombo, PR, Brazil. [20]Institute of Geography, Friedrich-Alexander-University Erlangen-Nuremberg, Wetterkreuz 15, 91058, Erlangen, Germany. [21]School of Geography, University of Leeds, Leeds, LS2 9JT, UK. [22]Fenner School of Environment and Society, Australian National University, Canberra, Australian Capital Territory, Australia. [23]Faculty of Environment and Resource studies, Mahidol University, 999 Phutthamonthon

Rd4, Salaya, Phutthamonthon, Nakhon Pathom 73170, Thailand. [24]Lamont-Doherty Earth Observatory, Columbia University, Palisades, New York, USA. [25]Instituto Pirenaico de Ecología (IPE-CSIC), E-50192 Zaragoza, Spain. [26]Instituto de Silvicultura e Industria de la Madera, Universidad Juárez del Estado de Durango, Durango 34120, Mexico. [27]Department of Botany, Institute of Biosciences, University of São Paulo, R. do Matão, 277, São Paulo, 05508-090, Brazil. [28]Instituto Nacional de Investigaciones Forestales, Agrícolas y Pecuarias (INIFAP), Centro Nacional de Investigación Disciplinaría en Relación Agua-Suelo-Planta-Atmósfera (CENID-RASPA), Margen Derecha del Canal del Sacramento Km 6.5, CP 35140, Gómez Palacio, Durango, Mexico. [29]Department of Environmental Technology and Management, Faculty of Environment, Kasetsart University, 50 Ngamwongwan Road, Jatujak District, Bangkok, 10900, Thailand. [30]CAS Key Laboratory of Tropical Forest Ecology, Xishuangbanna Tropical Botanical Garden, Chinese Academy of Sciences, Mengla, Yunnan, 666303, China. [31]School of Geography, Earth and Environmental Sciences, University of Birmingham, UK. [32]Birmingham Institute of Forest Research, University of Birmingham, UK. [33]Departamento Forestal, Universidad Autónoma Agraria Antonio Narro, Calzada Antonio Narro 1923, Buenavista CP 25315, Saltillo, Coahuila, Mexico. [34]Laboratory of Plant Anatomy and Dendrochronology, Department of Biology, Universidade Federal de Sergipe - UFS, Aracaju - SE, 49100-000, Brazil. [35]Laboratorio de Dendrocronología, Universidad Continental, Av. San Carlos 1980, Huancayo, Perú. [36]Department of Forest Sciences, Universidad Nacional de Colombia - Sede Medellín, Colombia. [37]Departamento de Agricultura, Biodiversidade e Florestas, Universidade Federal de Santa Catarina – UFSC, Curitibanos, Santa Catarina, Brazil. [38]TERRA Teaching and Research Centre, Gembloux Agro-Bio Tech, University of Liège, Gembloux, Belgium. [39]Master School for Carpentry and Cabinetmaking, Gleusdorfer Str. 14, D-96106 Ebern, Germany. [40]Department of Ecology and Evolutionary Biology, University of Arizona, Tucson, AZ 85721, USA. [41]Santa Fe Institute, 1399 Hyde Park Rd., Santa Fe, NM 87501, USA. [42]Department of Biological Sciences, University of Joinville Region - UNIVILLE, Joinville, SC, 89219-710, Brazil. [43]Postgraduate Program in Forestry, Regional University of Blumenau - FURB, Blumenau, SC, 89030-000, Brazil. [44]UR Forêts et Sociétés du CIRAD - Campus de Baillarguet TA C-22E, 34398 Montpellier cedex 5, France. [45]Gestion des Ressources Forestières de Gembloux Agro-Bio Tech,

ULiège, Passage des Déportés 2, 5030 Gembloux, Belgium. [46]Laboratorio de Dendrocronología e Historia Ambiental, IANIGLA, CCT-CONICET-Mendoza, Av. Ruiz Leal s/n, Parque Gral. San Martín, CC 330, CP 5500, Mendoza, Argentina. [47]Department of Crop Sciences, Tropical Plant Production and Agricultural Systems Modelling, Göttingen University, Grisebachstrasse 6, Göttingen, 37077, Germany. [48]School of Biological Sciences, University of Western Australia, Perth WA 6009, Australia. [49]USDA Forest Service, Pacific Southwest Research Station, Institute of Pacific Islands Forestry, Hilo, HI, USA. [50]Department of Forest Sciences, Federal University of Paraná, Curitiba - PR, Brazil. [51]World Agroforestry Centre (ICRAF), United Nations Avenue, P.O. Box 30677-00100, Nairobi, Kenya. [52]Facultad de Ingeniería, Tecnológico de Antioquia, Medellín, Colombia. [53]Natural Resources and Environmental Sciences Department, Forestry, Ecology and Wildlife Program, Alabama A&M University, Alabama, US. [54]Programa de Pós-Graduação em Agronomia/Fisiologia Vegetal, Departamento de Biologia, Instituto de Ciências Naturais, Universidade Federal de Lavras, 7203-202 Lavras, MG, Brazil. [55]Flanders Heritage Agency, Havenlaan 88 box 5, 1000 Brussels, Belgium. [56]Department of Earth and Spatial Sciences, University of Idaho, Moscow, ID, USA. [57]German Archaeological Institute DAI, Department of Natural Sciences, 14195, Berlin, Germany. [58]Geography Department, Humboldt-University Berlin, 12489, Berlin, Germany. [59]GFZ German Research Centre for Geosciences, 14473, Potsdam, Germany. [60]Faculty of Bioscience Engineering, Department of Environment, Laboratory of Wood Technology (UGent-Woodlab), Ghent University, Ghent, Belgium. [61]School of Biological Sciences, Washington State University, PO Box 644236, Pullman, WA 99164-4236, USA. [62]Faculty of Forestry and Wood Sciences, Czech University of Life Sciences Prague, Prague, Czech Republic. [63]U.S. Fish and Wildlife Service, Region 2, 500 Gold Ave. SW, PO BOX 1306, Albuquerque, NM 87103, USA. [64]Department of Ecology and Biogeography, Faculty of Biological and Veterinary Sciences, Nicolaus Copernicus University, Lwowska 1, 87-100, Toruń, Poland. [65]Centre for Climate Change Research, Nicolaus Copernicus University, ul. Lwowska 1, 87-100 Toruń, Poland. [66]Instituto Nacional de Innovación Agraria, Programa Nacional de Investigación Forestal, Hualahoyo km 8, Huancayo, Perú. [67]Department of Natural Resource Management, South Dakota State University, Brookings, SD, USA. [68]Department of Geography, Swansea University, Singleton Park, Swansea SA2 8PP, UK. [69]Department of Soils and Rural

Engineering, Faculty of Agronomy and Animal Science, Federal University of Mato Grosso - UFMT, Cuiabá, Mato Grosso, Brazil. [70]Center of Nuclear Energy in Agriculture, University of São Paulo, Av. Centenário 303, 13416-000, Brazil. [71]Department of Animal Science, Federal University of Paraná, Curitiba - PR, 80035-050, Brazil. [72]CITAB - Department of Forestry Sciences and Landscape (CIFAP), University of Trás-os-Montes and Alto Douro, Quinta de Prados, 5000-801, Vila Real, Portugal. [73]Plant Ecology, Institute of Integrative Biology, D-USYS, ETH-Zürich, 8006 Zürich, Switzerland. [74]Institute for Plant Sciences (IPS), University of Bern, 3013 Bern, Switzerland. [75]Department of Geography, Indiana University, Bloomington, IN, USA. [76]Facultad de Ciencias Naturales, Universidad Autónoma de Querétaro, Av. de las Ciencias s/n Juriquilla, CP 76230, Querétaro, Querétaro, Mexico. [77]Graduate Program in Ecology and Conservation, Federal University of Sergipe – UFS, São Cristóvão, Sergipe, Brazil. [78]Brazilian Agricultural Research Corporation (Embrapa), Embrapa Amazônia Ocidental, 69010-970, Manaus, AM, Brazil. [79]IHE Delft, P.O. Box 3015, 2601 DA Delft, The Netherlands. [80]VU University Amsterdam, De Boelelaan 1085, 1081 HV Amsterdam, The Netherlands. [81]Posgrado en Bosques y Conservación Ambiental, Universidad Nacional de Colombia, Medellín, Colombia. [82]Centro Universitario de Ciencias Biológicas y Agropecuarias, Universidad de Guadalajara, 45200 Zapopan, Jalisco, Mexico. [83]Centre for Functional Ecology, Department of Life Sciences, Faculty of Sciences and Technology, University of Coimbra, Portugal. [84]National Biobank of Thailand, National Science and Technology Development Agency, Pathum Thani 12120, Thailand. [85]Department of Biomaterials Science and Technology, School of Natural Resources, The Copperbelt University, P.O. Box 21692, Kitwe, Zambia. [86]Laboratory of Ecology and Dendrology, Federal Institute of Sergipe IFS, São Cristovão, Sergipe, 49100-000, Brazil. [87]Laboratory of Plant Ecology, Universidade do Vale do Rio dos Sinos (UNISINOS), Av. Unisinos, 950, Cristo Rei, São Leopoldo, RS, 93022-750, Brazil. [88]Instituto Biodiversa, Porto Alegre, RS, Brazil. [89]Nuclear Energy in Agriculture, University of São Paulo, Avenida Centenário, 303 - São Dimas, Piracicaba - SP, 13416-000, Brazil. [90]Department of Botany and Ecology, Institute of Biosciences, Federal University of Mato Grosso (UFMT), Cuiabá, Mato Grosso , Brazil. [91]Tree-Ring Laboratory, Lamont-Doherty Earth Observatory, Columbia University, 61 Route 9W, Palisades, NY 10964,USA. [92]Carrera de Ingeniería Forestal, Universidad Autónoma Gabriel René Moreno, Facultad

de Ciencias Agrícolas, Km 9 al Norte, El Vallecito, Santa Cruz, Bolivia. [93]BIOAPLIC, Departamento de Botánica, Universidade de Santiago de Compostela, EPSE, Campus Terra, 27002 Lugo, Spain. [94]El Colegio de la Frontera Sur, Departamento de Sociedad y Cultura, San Cristóbal de Las Casas, Chiapas, Mexico. [95]Escuela Profesional de Ingeniería Forestal de la Universidad Nacional Toribio Rodríguez de Mendoza de Amazonas, Calle Higos Urco N° 342, Chachapoyas, Perú. [96]Laboratorio de Dendrocronología, Carrera de Ingeniería Forestal, Universidad Nacional de Loja, 110101 Loja, Ecuador. [97]Department of Environmental Studies, University of California Santa Cruz, Santa Cruz, California, USA. [98]Facultad de Ciencias Agrarias, Universidad del Cauca, Popayán, Colombia. [99]Hémera Centro de Observación de la Tierra, Escuela de Ingeniería Forestal, Facultad de Ciencias, Universidad Mayor, Santiago, Chile. [100]Centro de Apoio Técnico à Execução Ambiental, Ministério Público do Estado de Mato Grosso. [101]Instituto Nacional de Investigaciones Forestales, Agrícolas y Pecuarias (INIFAP), Centro de Investigación Regional Pacífico Centro - Campo Experimental, Centro Altos de Jalisco, Jalisco, Mexico. [102]DendrOlavide, Departamento de Sistemas Físicos, Químicos y Naturales, Universidad Pablo de Olavide, Crta. de Utrera km. 1, 41013, Sevilla, Spain. [103]Forest and Nature Management, Van Hall Larenstein Univerisity of Applied Sciences, Velp, The Netherlands. [104]National Institute for Amazon Research, Av. André Araújo, 2.936, Petrópolis, CEP 69.067-375, Manaus, Amazonas, Brazil. [105]Environmental Studies, Department of Biology, Institute of Ecology and Evolution, University of Oregon, 97403-5223, Eugene, OR, USA. [106]Department of Earth Sciences, Freie Universität Berlin, Malteserstraße 74-100, 12249 Berlin, Germany. [107]Instituto de Ecología Aplicada, Universidad Autónoma de Tamaulipas, Av. División del Golfo No 356, Col. Libertad, CP 87020, Ciudad Victoria, Tamaulipas, Mexico. [108]Institute of Biodiversity and Forests, Federal University of Western Pará - UFOPA, Santarém - PA, 68040-255, Brazil. [109]Department of Earth and Environmental Systems, Indiana State University, Science 159E, Terre Haute, IN, 47809, USA. [110]Department of Geography, University of Alabama, Tuscaloosa, AL, USA. [111]Programa de Investigación de Ecología y Biodiversidad, Asociación ANDINUS, Calle Miguel Grau 370, Sicaya, Huancayo, Junín, Peru. [112]Department of Geography, Johannes Gutenberg University, Mainz, Germany. [113]Department of Environmental Science, Faculty of Science, Chulalongkorn University, Bangkok, 10330, Thailand. [114]Water Science and Technology for Sustainable Environment Research

Unit, Chulalongkorn University, Bangkok, 10330, Thailand. [115]Instituto de Geografía, Universidad Nacional Autónoma de Mexico, Ciudad Universitaria, Mexico City, 04510, Mexico. [116]Facultad de Ciencias Forestales, Colegio de Postgraduados, Montecillos, Texcoco, Mexico. [117]Instituto de Ciencias Agroalimentarias, Animales y Ambientales (ICA3), Universidad de O'Higgins, San Fernando, Chile. [118]Biological Sciences Department, California State University, San Marcos (CSUSM), CA, USA. [119]Faculty of Civil Engineering and Geosciences, Delft University of Technology, Delft, The Netherlands. [120]School of Teacher Training for Secondary Education Tilburg, Fontys University of Applied Sciences, Tilburg, The Netherlands. [121]Department of Ecology and Evolutionary Biology, University of California, Santa Cruz, Santa Cruz, CA, USA. [122]School of Earth Sciences, Addis Ababa University, Addis Ababa, Ethiopia. [123]School of Biology and Ecology, University of Maine, Orono, ME 04469, USA. [124]School of Natural Resources and the Environment, University of Arizona, Tucson, AZ, USA.

* Corresponding author. Email: pieter.zuidema@wur.nl

Abstract:

Increasing drought pressure under anthropogenic climate change may jeopardize the potential of tropical forests to capture carbon in woody biomass and act as a long-term CO_2 sink. To evaluate this risk, we assessed drought impacts in 483 tree-ring chronologies from across the tropics and found an overall modest stem growth decline (2.5%, 95% confidence interval 2.2-2.7%) during the 10% driest years since 1930. Stem growth declines exceeded 10% in a quarter of cases, were larger at hotter and drier sites, and for gymnosperms compared to angiosperms. Growth declines generally did not outlast drought years and were partially mitigated by growth stimulation in wet years. Thus, pantropical forest carbon sequestration through stem growth has hitherto shown drought resilience that may, however, diminish under future climate change.

Main Text:

Tropical forests and woodlands are key components of the global carbon cycle. They represent much of the carbon stocks in terrestrial vegetation, contribute strongly to the land carbon sink, and are a key driver of the interannual variation in this sink (*1, 2*). The long-term capture and storage of carbon in tropical woody biomass has a high potential to contribute to nature-based solutions to climate change by acting as a CO_2 sink (*3, 4*). However, the increasing incidence and intensity of droughts may fundamentally alter these services (*5-8*), temporarily shifting tropical vegetation to a net carbon source (*5, 7, 9*), and jeopardizing its role in climate change mitigation (*10*). Droughts can be due to low precipitation (P), high atmospheric water demand (vapor pressure deficit, VPD) or both simultaneously, leading to strong climatic water deficit (CWD, water demand minus supply). Each of these drought types may reduce tropical tree growth.

To understand and predict the risks that droughts pose for the long-term capture of carbon in tropical vegetation, a pantropical assessment of drought effects on stem growth is needed. Yet, studies of drought effects on tree growth are scarce and poorly replicated spatially (*11-13*). This situation reduces possibilities to generalize and contextualize local empirical findings and to validate terrestrial biosphere models, which currently poorly represent the formation (*14, 15*) and climate sensitivity of tropical woody biomass (*16*). These modelling uncertainties are bound to persist unless constrained by extensive empirical studies.

Here, we leverage the recent expansion of tropical tree-ring studies (*17, 18*) to assess drought effects on stem growth at an annual resolution and over multi-decadal time scales. We assembled the most extensive pantropical tree-ring network to date, extending across all tropical climates, to answer the following questions: (i) To what extent is stem growth reduced during drought years and does this differ across drought types (i.e., low P; high VPD; high CWD), seasons (i.e., dry vs. wet), and major clades (i.e., angiosperms vs. gymnosperms)? (ii) Is there evidence for lagged drought effects on stem growth and – if so – how strong or persistent are these lag effects? (iii) To what extent does growth stimulation during wet extremes compensate for stem growth reduction during droughts? (iv) Does the magnitude of drought impacts depend on local climatic conditions? Based on knowledge about

growth-limiting factors and results from extra-tropical tree-ring studies, we hypothesize drought effects to be stronger for CWD droughts than for P and VPD droughts, for gymnosperms than for angiosperms (question i; *19, 20*), lag effects to exist, especially for gymnosperms (question ii; *19, 21*), drought-induced growth declines to be partially compensated by growth stimulation during wet extremes (question iii; *22, 23*) and drought effects to be stronger in more arid regions (question iv; *19, 23*).

Pantropical tree-ring network

We compiled a network of 483 tree-ring width chronologies from >10,000 trees spanning tropical and subtropical latitudes (30°N-30°S). This dataset comprises 163 species and 33 plant families, with similar proportions of angiosperm and gymnosperm chronologies (Fig. 1A, fig. S1). Chronologies were re-developed from >20,000 time series of raw tree ring-width measurements, using a single flexible detrending procedure that retains short-term growth responses to climate extremes. The resulting ring-width index (RWI) chronologies represent a relative, population-level measure of tree-growth variability. For each site, we identified the 10% driest years (since 1930) in terms of precipitation (P, lowest values), VPD (highest values), and CWD (highest values) in either the wet or dry season. CWD was calculated as cumulative abs(P-PET) for months during the season when PET>P (PET=Potential Evapotranspiration). We studied droughts at the seasonal level because the climate sensitivity of tropical tree growth differs among seasons (*17*). We quantified impacts of droughts (and wet extremes on RWI using Superposed Epoch Analysis (SEA, *24*), a technique that compares the mean RWI anomaly in drought years with that of random draws from all "normal" years in the chronology, and tests significant deviations (*21*). We estimated lag effects during the first and second post-drought years. We used the same procedure to study effects of wet extremes. RWI anomalies provide robust site-level estimates of drought impacts and can be interpreted as proportional reductions in stem diameter growth (fig. S2); we thus refer to them as 'growth anomalies' or 'growth reductions' (when negative). To account for the higher abundance of tree-ring studies at high

elevations and in arid climates (fig. S3), we present pantropical medians weighted by climatic representativeness.

The drought intensity of the selected 10% driest years (expressed as number of standard deviations away from the long-term mean) was comparable across the three drought types (fig. S4). Overlap in event years across drought types was small, except for dry-season extremes in P and CWD (fig. S5), suggesting that CWD droughts are more driven by very low P than by very high VPD. Across drought types and seasons, 7% of the droughts occurred during two consecutive years, and 0.3% lasted for three years. Since 1930, the frequency of droughts has increased for all drought types (fig. S6A), while the intensity has increased for some (VPD and CWD), but decreased for others (P, fig. S6B).

Variable but overall modest drought effects

Growth anomalies during the 10% driest years were predominantly negative (63% of incidences), with strong growth reductions (>10%) occurring in a quarter of the chronologies. Yet, growth anomalies varied across the network from strongly negative to moderately positive (fig. S7A) and growth anomaly variations were stronger for individual drought years (fig. S6C) than for averages across drought years. This wide variety of growth anomalies during individual drought years fully captures previously reported responses of tropical trees to episodic droughts, ranging from stem growth reductions of 20-50% (*25, 26*) to undetectable change (*13, 27*) or growth increases (for small trees, *28*). The latter may result from reduced cloudiness, enhanced leaf production, and/or competitive release in humid regions (*28, 29*).

Despite the large variation in site-specific drought responses, bootstrapped 95% confidence intervals (CI) of the weighted median responses were narrow (Fig. 1B). Overall, the magnitude of growth declines during drought years was modest (Fig. 1B). The pantropical growth reduction for all drought types and seasons was 2.5% (weighted median, CI: 2.2-2.7%, angiosperms and gymnosperms combined). Growth reduction was significantly stronger for dry-season droughts (3.1%, CI: 2.8-3.5%) than wet-season droughts (1.8%; CI: 1.6-2.1%; Mann Whitney U test, $p<0.001$). Our assessments

focuses at the pantropical level, because continental-level comparisons are hampered by differences in climatic representation (Fig. S1D) and local-scale assessments by high local tree diversity (Fig. S1E).

A quarter of the growth anomalies during dry-season droughts and 15% during wet-season droughts were significant ($p<0.05$; Fig. 1B, fig. S7A). SEA analyses of individual ring-width series revealed smaller proportions of significant growth declines: 10% during the dry season and 7% during the wet season (fig. S8). These lower percentages likely reflect a larger role of non-climatic factors in inducing growth variation of individual trees (e.g., canopy disturbance, carry-over effects) than at the population level.

Applying a more stringent selection of drought years (i.e., the 5% driest years) led to a somewhat stronger – but still modest – mean reduction of 3.2% (CI: 2.7-3.5%). This modest drought response is comparable in magnitude to that from multi-site assessments in tropical forests, which reported 6-9% reduction in diameter growth or woody biomass productivity (*11, 30, 31*). The stronger growth reductions in those studies may be explained by the selection of more extreme droughts.

Drought responses differed markedly between angiosperms and gymnosperms (Fig. 1B). Dry-season droughts induced significantly stronger growth reductions for gymnosperms (4.4%; CI: 4.0-5.1%) than for angiosperms (1.1%; CI: 0.5-1.9%, Table S1). By contrast, wet-season droughts resulted in stronger growth declines for angiosperms (2.7%; CI: 2.2-3.1%) than gymnosperms (1.3%; CI: 0.8-1.6%; Table S1). Stronger drought responses of gymnosperms are broadly consistent with the results of extra-tropical tree-ring studies (*19, 21, 22, 32*). These taxonomic differences cannot be explained by the drought intensity, which was similar for angiosperms and gymnosperms (fig. S4). Possible explanations of stronger drought effects for gymnosperms include a dominant evergreen leaf phenology (89% of gymnosperm chronologies), an inherently stronger growth variability (*21*), a stronger vulnerability to cavitation for *Pinaceae* (80% of our chronologies) (*33*), and lower concentrations of non-structural carbohydrate (NSC) reserves (*34*). The marked differences in drought responses and hydraulic architecture between angiosperms and gymnosperms call for separate drought analyses of these major clades.

312 In contrast to our hypothesis (i), growth reductions were not larger during CWD droughts compared to
313 P or VPD droughts (Fig. 1B, Table S1). This may partially be explained by the high coincidence of
314 CWD and P droughts (fig. S5), resulting in similar effects on tree growth.

315

316 **Rapid post-drought recovery**

317 Contrary to our hypothesis (ii) , drought analyses revealed no evidence for strong or long-lasting lag
318 effects for any drought type or season (Fig. 2). Compared to drought years, post-drought years
319 exhibited significantly smaller negative growth anomalies, and anomalies often shifted to positive.
320 Such significant changes were found in 80% of the 36 possible comparisons (of clades, seasons, and
321 drought types) between drought and post-drought years. During post-drought years, the confidence
322 intervals of growth anomalies included zero or were fully above zero for 70% of the 36 combinations
323 of drought types, seasons and clades. Post-drought recovery was similar for angiosperms and
324 gymnosperms (Fig. 2) and cannot be explained by post-drought climatic conditions, which are close to
325 normal or only slightly wetter (fig. S4B-C).

326 Robustness tests revealed that these drought responses do not shift when applying more rigid
327 detrending methods (fig. S9), alternative climate products (fig. S10, S11), more stringent drought
328 selection criteria (fig. S12A-B) or when selecting two-year droughts (fig. S12C).

329 Combined, our results point to a rapid recovery of tree growth to pre-drought levels and provide no
330 evidence for the existence of strong or long lag effects at the pantropical scale. These results are
331 consistent with the short (<18 months) lag effects in tree growth after droughts observed in tropical
332 dendrometer studies (*11*, *35*) and extra-tropical tree-ring studies (*22*). Yet, our results contrast with the
333 strong lagged drought responses for gymnosperms observed in a tree-ring study across extra-tropical
334 sites (*19*), likely due to differences in site aridity, drought definitions, detrending methods, and species
335 selection (*22*).

336

Drought effects are partially mitigated by wet extremes

To contextualize drought-induced growth anomalies, we compared the overall effect of the 10% driest years on tree growth to growth changes during the 10% wettest years (SEA analysis). As hypothesized (iii), these wettest years caused pantropical tree growth to increase (median 1.8%; CI: 1.5-2.0%; fig. S7B), a magnitude that is comparable to the 2.5% drought-induced growth reduction (Fig. 1B). Similar to drought responses, growth anomalies following wet extreme years were short-lived (fig. S13).

As a result of the growth increases during extreme wet years, net growth anomalies of the 10% driest and wettest years combined were overall very small (-0.4%; CI: -0.2 to -0.5%) and not significantly different from zero for most drought types (Fig. 3). Yet, wet extremes mitigated only half (47%; CI: 43-52%) of the growth reduction during drought years (across seasons, drought types, and for angiosperms and gymnosperms combined; Fig. 3). However, with increasing frequency or severity of droughts (fig S6A-B) and in more arid conditions (*23*), this wet-year compensation may be reduced.

Drought impacts increase with aridity

We evaluated the climatic drivers of observed drought effects by interpolating growth anomalies across climate space (mean annual precipitation and temperature). We find that wet-season droughts reduced growth in angiosperms more strongly in hotter and more arid climates (Fig. 4A, fig. S14A, S15A), whereas dry-season droughts had stronger impacts on gymnosperms at more arid sites (Fig. 4A, fig. S14B, S15B). Path analyses yielded consistent results (fig. S16) and also revealed that the expected role of first-order growth autocorrelation in shaping drought effects (*22*) was very small. Our finding of aggravating drought effects with increasing aridity is consistent with those from earlier studies on tropical (*36*) and extra-tropical (*19, 20, 23, 37*) tree species. Strong local variability in drought responses is commonly found (*35*), likely due to interspecific differences in drought resistance (*38*), spatial variation in soil parameters, rooting depth, access to water (*39*), and variation in the timing, intensity, and duration of droughts (*37*).

We projected the climate-space patterns for growth anomalies during low-precipitation years (models with highest R^2) into geographic space (Fig. 4B). For angiosperms, this model suggests that the strongest drought-induced growth reductions occur in dry-forest biomes in the Americas, Africa, Southern Asia, and Eastern Australia. Modest or positive drought effects on stem growth are estimated in warm-humid zones such as the Amazon region. For gymnosperms, negative growth anomalies due to dry-season droughts are strong throughout high-elevation regions in the Americas, Asia, and eastern Africa. Despite large local variability in drought responses, the bootstrapped uncertainty of these maps is low (fig. S17). Thus, across major climatic gradients at the sub-continental scale, predicted distributions of drought responses likely hold. These results offer opportunities to benchmark and constrain simulated drought responses of woody biomass production in tropical forests by terrestrial biosphere models (*16, 40*).

Drought responses across components of productivity

The drought effects on stem growth are smaller than those on leaf-level photosynthesis (*31*) and forest-level Gross Primary Productivity (GPP) (*13*), but of comparable magnitude to effects on leaf fall, flushing, and mature leaf area (*35*). In terms of duration, drought impacts on stem growth tend to last somewhat longer (4-18 months) (*27, 35*) than effects on GPP (typically 4-6 months) (*41, 42*). These comparisons suggest more direct and stronger drought effects on carbon uptake through photosynthesis than on its sequestration in woody biomass, in line with decoupling of these processes observed in extra-tropical forests (*43*).

One of the plausible explanations of the observed drought resilience of tropical tree growth is the mobilization of non-structural carbohydrates (NSC). Tropical tree species store large amounts of starch and soluble sugars in stems, branches, roots, and leaves (*44*) that are available during dry episodes for osmoregulation, leaf flushing and stem growth (*13, 34, 45, 46*). NSC mobilization may buffer reductions in stem growth and explain the decoupling of canopy and stem responses to droughts, but remains poorly quantified. Other mechanisms, including shifts in phenology, structure

388 and stem hydraulics (*47*) may also contribute to drought resilience. Long-term, well-replicated field
389 studies measuring functional and productivity changes are needed.

390

391 **Limitations, mortality risks and climate change**

392 We acknowledge several limitations of our study that should be addressed in future studies. First,
393 major sampling gaps exist in Africa and in extreme arid and humid climates (figs S1, S3) (*18*). While
394 we statistically account for biases, data scarcity can only be solved through new studies. Second, our
395 chronologies only include cross-dated RWI series and our study thus may have excluded individuals
396 that did not cross-date due to extraordinarily strong (e.g., missing rings) or weak drought responses.
397 The latter group of individuals may produce progeny for drought-resilient next generations, if weak
398 responses have a genetic basis. Third, our study species represent a small fraction of tropical tree
399 richness and their drought responses may somewhat deviate from that of the 'average' tropical species.
400 Finally, we do not quantify drought responses at the stand level. Upscaling from tree- to forest-level
401 would require comparing tree-ring based responses with those from community-wide dendrometer or
402 plot data.

403 Episodic droughts increase mortality of tropical trees (*6, 48*). Drought-induced stem growth reductions
404 may be associated with elevated mortality. To provide a first estimate of mortality risks associated
405 with the growth reductions reported here for angiosperms, we used significant growth-mortality
406 associations from 10 tropical forest field studies (*49*) (fig. S18A-B). The resulting estimate is a first
407 indication of the order of magnitude of additional tree mortality. We estimate this to be 0.1% y^{-1} (CI:
408 0.08-0.15%) on top of a 1% y^{-1} baseline (fig. S18C). The resulting carbon loss of this additional
409 mortality may be substantial at the pantropical scale and likely recovers slowly (*50*).

410 Anthropogenic climate change has intensified drought stress (fig. S6A-B), resulting in stronger
411 drought-induced growth reductions for all drought types (fig. S6C). Future climate change will further
412 increase the frequency of droughts in tropical forests (*51, 52*). Our climate space interpolation and path
413 analyses suggest that future warming and amplified climatic variability will cause stronger stem-

414 growth declines during wet-season droughts in angiosperm-dominated tropical lowland forests and
415 woodlands. For gymnosperm-dominated high-elevation forests, stronger impacts of dry-season
416 droughts are expected in regions where climate change would reduce precipitation. These shifts are
417 unlikely to be mitigated by concurrent CO_2 rise (*9*), because no consistent CO_2-induced growth
418 stimulation has been observed in tree-ring studies (*53*).

419 Stronger and more extensive droughts occurring under future climate change may shift the modest
420 drought responses observed here for the past decades toward considerably larger and more widespread
421 declines in tropical wood productivity. Such shifts may have implications for the dynamics and
422 residence time of carbon in tropical forests, especially when stronger growth reductions are
423 accompanied by increasing tree mortality.

424

References and Notes:

1. Y. Pan *et al.*, A large and persistent carbon sink in the world's forests. *Science* **333**, 988-993 (2011).
2. P. Friedlingstein *et al.*, Global Carbon Budget 2019. *Earth System Science Data* **11**, 1783-1838 (2019).
3. A. Koch, J. O. Kaplan, Tropical forest restoration under future climate change. *Nature Climate Change* **12**, 279-+ (2022).
4. B. Buma *et al.*, Expert review of the science underlying nature-based climate solutions. *Nature Climate Change* **14**, 402-406 (2024).
5. N. G. McDowell *et al.*, Pervasive shifts in forest dynamics in a changing world. *Science* **368**, eaaz9463 (2020).
6. P. M. Brando *et al.*, Droughts, Wildfires, and Forest Carbon Cycling: A Pantropical Synthesis. *Annu Rev Earth Pl Sc* **47**, 555-581 (2019).
7. D. M. Lapola *et al.*, The drivers and impacts of Amazon forest degradation. *Science* **379**, eabp8622 (2023).
8. W. Yuan *et al.*, Increased atmospheric vapor pressure deficit reduces global vegetation growth. *Science Advances* **5**, eaax1396 (2019).
9. J. Penuelas *et al.*, Shifting from a fertilization-dominated to a warming-dominated period. *Nature Ecology & Evolution* **1**, 1438-1445 (2017).
10. W. R. L. Anderegg *et al.*, Climate-driven risks to the climate mitigation potential of forests. *Science* **368**, eaaz7005 (2020).
11. S. W. Rifai *et al.*, ENSO Drives interannual variation of forest woody growth across the tropics. *Philos. Trans. R. Soc. Lond. B Biol. Sci.* **373**, 20170410 (2018).
12. P. M. Brando *et al.*, Drought effects on litterfall, wood production and belowground carbon cycling in an Amazon forest: results of a throughfall reduction experiment. *Philos. Trans. R. Soc. Lond. B Biol. Sci.* **363**, 1839-1848 (2008).
13. C. E. Doughty *et al.*, Drought impact on forest carbon dynamics and fluxes in Amazonia. *Nature* **519**, 78-82 (2015).
14. P. A. Zuidema, B. Poulter, D. C. Frank, A Wood Biology Agenda to Support Global Vegetation Modelling. *Trends in Plant Science* **23**, 1006-1015 (2018).
15. F. Babst *et al.*, Modeling Ambitions Outpace Observations of Forest Carbon Allocation. *Trends in Plant Science* **26**, 210-219 (2021).
16. X. Xu *et al.*, Constraining long-term model predictions for woody growth using tropical tree rings. *Glob. Chang. Biol.* **30**, e17075 (2024).
17. P. A. Zuidema *et al.*, Tropical tree growth driven by dry-season climate variability. *Nature Geoscience* **15**, 269-276 (2022).
18. P. Groenendijk *et al.*, The importance of tropical tree-ring chronologies for global change research. *Quaternary Science Reviews* **355**, 109233 (2025).
19. W. R. L. Anderegg *et al.*, Pervasive drought legacies in forest ecosystems and their implications for carbon cycle models. *Science* **349**, 528-532 (2015).
20. A. Gazol, J. J. Camarero, W. R. L. Anderegg, S. M. Vicente-Serrano, Impacts of droughts on the growth resilience of Northern Hemisphere forests. *Global Ecology and Biogeography* **26**, 166-176 (2017).
21. A. Gazol *et al.*, Drought legacies are short, prevail in dry conifer forests and depend on growth variability. *J. Ecol.* **108**, 2473-2484 (2020).
22. S. Klesse *et al.*, Legacy effects in radial tree growth are rarely significant after accounting for biological memory. *J. Ecol.* **111**, 1188-1202 (2022).
23. M. P. Dannenberg, E. K. Wise, W. K. Smith, Reduced tree growth in the semiarid United States due to asymmetric responses to intensifying precipitation extremes. *Science Advances* **5**, eaaw0667 (2019).

24. J. M. Lough, H. C. Fritts, An assessment of the possible effects of volcanic eruptions on North American climate using tree-ring data, 1602 to 1900 A.D. *Climatic Change* **10**, 219-239 (1987).
25. M. Rahman, M. Islam, A. Bräuning, Species-specific growth resilience to drought in a mixed semi-deciduous tropical moist forest in South Asia. *For. Ecol. Manage.* **433**, 487-496 (2019).
26. D. B. Clark, D. A. Clark, S. F. Oberbauer, Annual wood production in a tropical rain forest in NE Costa Rica linked to climatic variation but not to increasing CO2. *Glob. Chang. Biol.* **16**, 747-759 (2010).
27. J. A. Hogan *et al.*, Drought and the interannual variability of stem growth in an aseasonal, everwet forest. *Biotropica* **51**, 139-154 (2019).
28. A. C. Bennett, N. G. McDowell, C. D. Allen, K. J. Anderson-Teixeira, Larger trees suffer most during drought in forests worldwide. *Nature Plants* **1**, 15139 (2015).
29. L. Rowland *et al.*, Death from drought in tropical forests is triggered by hydraulics not carbon starvation. *Nature* **528**, 119-122 (2015).
30. T. R. Feldpausch *et al.*, Amazon forest response to repeated droughts. *Global Biogeochemical Cycles* **30**, 964-982 (2016).
31. T. Janssen, K. Fleischer, S. Luyssaert, K. Naudts, H. Dolman, Drought resistance increases from the individual to the ecosystem level in highly diverse Neotropical rainforest: a meta-analysis of leaf, tree and ecosystem responses to drought. *Biogeosciences* **17**, 2621-2645 (2020).
32. X. Li *et al.*, Temporal trade-off between gymnosperm resistance and resilience increases forest sensitivity to extreme drought. *Nature Ecology & Evolution* **4**, 1075-1083 (2020).
33. B. Choat *et al.*, Global convergence in the vulnerability of forests to drought. *Nature* **491**, 752-755 (2012).
34. J. Martínez-Vilalta *et al.*, Dynamics of non-structural carbohydrates in terrestrial plants: a global synthesis. *Ecol. Monogr.* **86**, 495-516 (2016).
35. T. Janssen *et al.*, Drought effects on leaf fall, leaf flushing and stem growth in the Amazon forest: reconciling remote sensing data and field observations. *Biogeosciences* **18**, 4445-4472 (2021).
36. D. Bauman *et al.*, Tropical tree growth sensitivity to climate is driven by species intrinsic growth rate and leaf traits. *Glob. Chang. Biol.* **28**, 1414-1432 (2022).
37. X. C. Wu *et al.*, Timing and Order of Extreme Drought and Wetness Determine Bioclimatic Sensitivity of Tree Growth. *Earth's Future* **10**, (2022).
38. R. S. Oliveira *et al.*, Linking plant hydraulics and the fast-slow continuum to understand resilience to drought in tropical ecosystems. *New Phytologist* **230**, 904-923 (2021).
39. N. B. Schwartz *et al.*, Topography and Traits Modulate Tree Performance and Drought Response in a Tropical Forest. *Frontiers in Forests and Global Change* **3**, (2020).
40. S. Klesse *et al.*, A Combined Tree Ring and Vegetation Model Assessment of European Forest Growth Sensitivity to Interannual Climate Variability. *Global Biogeochemical Cycles* **32**, 1226-1240 (2018).
41. Z. Zhang, W. Ju, Y. Zhou, X. Li, Revisiting the cumulative effects of drought on global gross primary productivity based on new long-term series data (1982-2018). *Glob. Chang. Biol.* **28**, 3620-3635 (2022).
42. J. Yang *et al.*, Amazon drought and forest response: Largely reduced forest photosynthesis but slightly increased canopy greenness during the extreme drought of 2015/2016. *Glob. Chang. Biol.* **24**, 1919-1934 (2018).
43. A. Cabon *et al.*, Cross-biome synthesis of source versus sink limits to tree growth. *Science* **376**, 758-761 (2022).
44. M. K. Wurth, S. Pelaez-Riedl, S. J. Wright, C. Korner, Non-structural carbohydrate pools in a tropical forest. *Oecologia* **143**, 11-24 (2005).
45. L. T. Dickman *et al.*, Homoeostatic maintenance of nonstructural carbohydrates during the 2015-2016 El Nino drought across a tropical forest precipitation gradient. *Plant Cell Environ.* **42**, 1705-1714 (2019).

46. C. Signori-Müller *et al.*, Non-structural carbohydrates mediate seasonal water stress across Amazon forests. *Nat. Commun.* **12**, 2310 (2021).
47. J. V. Tavares *et al.*, Basin-wide variation in tree hydraulic safety margins predicts the carbon balance of Amazon forests. *Nature*, (2023).
48. W. M. Hammond *et al.*, Global field observations of tree die-off reveal hotter-drought fingerprint for Earth's forests. *Nat. Commun.* **13**, 1761 (2022).
49. S. E. Russo *et al.*, The interspecific growth-mortality trade-off is not a general framework for tropical forest community structure. *Nature Ecology & Evolution* **5**, 174-183 (2021).
50. J. P. Wigneron *et al.*, Tropical forests did not recover from the strong 2015-2016 El Nino event. *Science Advances* **6**, eaay4603 (2020).
51. C. G. Xu *et al.*, Increasing impacts of extreme droughts on vegetation productivity under climate change. *Nature Climate Change* **9**, 948-+ (2019).
52. S. Saatchi *et al.*, Detecting vulnerability of humid tropical forests to multiple stressors. *One Earth* **4**, 988-1003 (2021).
53. A. P. Walker *et al.*, Integrating the evidence for a terrestrial carbon sink caused by increasing atmospheric CO2. *New Phytologist* **229**, 2413-2445 (2021).
54. P. A. Zuidema *et al.*, Data and Code associated with original research article: Pantropical tree rings show small effects of drought on stem growth (2025) https://doi.org/10.5061/dryad.hx3ffbgq4
55. International Tree-Ring Data Bank (ITRDB) (2025) https://www.ncei.noaa.gov/products/paleoclimatology/tree-ring
56. J. Liang *et al.*, Co-limitation towards lower latitudes shapes global forest diversity gradients. *Nature Ecology & Evolution* **6**, 1423-1437 (2022).
57. J. R. V. Aragão, P. A. Zuidema, P. Groenendijk, Climate-growth relations of congeneric tree species vary across a tropical vegetation gradient in Brazil. *Dendrochronologia* **71**, 125913 (2022).
58. R Core Team. (R Foundation for Statistical Computing, Vienna, Austria., 2024), vol. http://www.R-project.org/.
59. A. G. Bunn, A dendrochronology program library in R (dplR). *Dendrochronologia* **26**, 115-124 (2008).
60. S. E. Fick, R. J. Hijmans, WorldClim 2: new 1-km spatial resolution climate surfaces for global land areas. *International Journal of Climatology* **37**, 4302-4315 (2017).
61. I. Harris, T. J. Osborn, P. Jones, D. Lister, Version 4 of the CRU TS monthly high-resolution gridded multivariate climate dataset. *Sci Data* **7**, 109 (2020).
62. L. U. Castruita-Esparza *et al.*, Coping With Extreme Events: Growth and Water-Use Efficiency of Trees in Western Mexico During the Driest and Wettest Periods of the Past One Hundred Sixty Years. *Journal of Geophysical Research-Biogeosciences* **124**, 3419-3431 (2019).
63. P. A. Zuidema *et al.*, Recent CO2 rise has modified the sensitivity of tropical tree growth to rainfall and temperature. *Glob. Chang. Biol.* **26**, 4028-4041 (2020).
64. C. Ols *et al.*, Detrending climate data prior to climate–growth analyses in dendroecology: A common best practice? *Dendrochronologia* **79**, 126094 (2023).
65. J. T. Abatzoglou, S. Z. Dobrowski, S. A. Parks, K. C. Hegewisch, TerraClimate, a high-resolution global dataset of monthly climate and climatic water balance from 1958–2015. *Sci Data* **5**, 170191 (2018).
66. H. Hersbach *et al.*, The ERA5 global reanalysis. *Quarterly Journal of the Royal Meteorological Society* **146**, 1999-2049 (2020).
67. V. Trouet, G. L. Harley, M. Dominguez-Delmas, Shipwreck rates reveal Caribbean tropical cyclone response to past radiative forcing. *Proc. Natl. Acad. Sci. U. S. A.* **113**, 3169-3174 (2016).
68. A. E. Zanne *et al.*, Data from: Towards a worldwide wood economics spectrum (2009) https://doi.org/10.5061/dryad.234

69. Y. Rosseel, lavaan: An R Package for Structural Equation Modeling. *Journal of Statistical Software* **48**, 1-36 (2012).
70. F. Babst *et al.*, Twentieth century redistribution in climatic drivers of global tree growth. *Science Advances* **5**, eaat4313 (2019).
71. S. Chamberlain *et al.*, in *rgbif: Interface to the Global Biodiversity Information Facility API*. (2021).
72. A. T. Trugman *et al.*, Tree carbon allocation explains forest drought-kill and recovery patterns. *Ecol. Lett.* **21**, 1552-1560 (2018).
73. L. DeSoto *et al.*, Low growth resilience to drought is related to future mortality risk in trees. *Nat. Commun.* **11**, 545 (2020).
74. M. Cailleret *et al.*, A synthesis of radial growth patterns preceding tree mortality. *Glob. Chang. Biol.* **23**, 1675-1690 (2017).
75. A. Esquivel-Muelbert *et al.*, Tree mode of death and mortality risk factors across Amazon forests. *Nat. Commun.* **11**, 5515 (2020).
76. S. J. Davies *et al.*, ForestGEO: Understanding forest diversity and dynamics through a global observatory network. *Biol. Conserv.* **253**, 108907 (2021).

Acknowledgments:

Support and assistance: Smithsonian Tropical Research Institute-Panama, Sebastian Bernal (RaAS), Supervision: Helene Muller-Landau, S. Joseph Wright (RaAS), Fieldwork support: COOMFLONA - FLONA TAPAJÓS, Universidade do Oeste do Pará (BH), Sutó Company and Angel Chavez at Consultora Forestal Bosques e Industria (KPV), Logging company AMATA (DROR), Lab support: Rebecca Franklin, Guillermo Guada, Quirine Hakkaart, Annemarijn Nijmeijer and Peter van der Sleen (KPV). All data are available in the manuscript, the supplementary material or deposited at DataDryad (*54*).

Funding

AECID grant 11-CAP2-1730 (JJC)
Agencia Nacional de Promoción Científica y Tecnológica, Argentina grant PICT 2014-2797 (MEF)
Agencia Nacional de Promoción Científica y Tecnológica, Argentina grant PICT 2019-01336 (MEF)
BBVA Foundation (JJC)
Belspo BRAIN grant BR/143/A3/HERBAXYLAREDD (HB)
CAPES - Coordenação de Aperfeiçoamento de Pessoal de Nível Superior (TLS)
CAPES grant 88887.199858/2018-00 (GAP)
CAPES grant 88887.495294/2020-00 (BH)
CAPES. (PG)
CAPES/PDSE grant 15011/13-5 (MAP)
CGIAR (MM)
CNPq (CRA, FG, CSL, FAL, ASR)
CNPq 140849/2015-7 (AKM)
CNPq ENV grant FRG 0339638 (OD)
CNPq grant 1009/4785031-2 (GC)
CNPq grant 140277/2024-2 (DBCC)
CNPq grant 311247/2021-0 (JS)
CNPq grant 405923/2021-0 (MCS)
CNPq grant 406062/2023-4 (MCS)
CNPq grant 441811/2020-5 (JS)
CNPq grnat PQ 313129/2022-3 (ACB)
CONACYT Consejo Nacional de Ciencia y Tecnología México. Master fellowship (MILH)
CONACYT grant CB2016-283134 (JVD)
CONACYT grant CB-2016-283134 (LRCE)
CONAFOR-CONACYT grant C01-234547 (JCP)
CONAFOR-CONACYT grant CONAFOR-2014 (LRCE)
CONCYTEC Peru & World Bank grant 043-2019-FONDECYT-BM-INC.INV (JGI)
CONICET (FAR)
CONICET grant PIP-11220200102929CO (MEF)
Coordenação de Aperfeiçoamento de Pessoal de Nível Superior (EAF)
Copel Geração e Transmisão S.A. grant PD-06491-0405-2015 (AKM)
CUOMO Foundation (MM)
DAAD (MI)
Deutsche Forschungsgemeinschaft (DFG) (AA)
DFG grant BR 1895/15-1 (AB)
DFG grant BR 1895/23-1 (AB)
DFG grant BR 1895/29-1 (AB)
Dirección de Investigación de la Universidad Nacional de Loja (DPC)

Dirección General de Asuntos del Personal Académico of the UNAM (Mexico) (RB)
Estudios dendrocronológicos en las Sierras Madre Occidental, Oriental y del Sur de México, grant 38111-4251030012346 (ECO)
FACEPE grant IBPG-1418-5.00/21 (DBCC)
FAPEAM grant 01.02.016301.02630/2022-76 (JS)
FAPEMAT (FAL)
FAPEMIG grant APQ-01544-22 (ACB)
FAPEMIG grant APQ-02541-14 (GAP)
FAPESC grant 2019TR65 (TABF)
FAPESP grant 12/50457-4 (GC)
FAPESP grant 2009/53951-7 (MTF)
FAPESP grant 2017/50085-3 (GC, GML & DROR)
FAPESP grant 2018/01847-0 (PG)
FAPESP grant 2018/07632-6 (MGV)
FAPESP grant 2018/22914-8 (DROR)
FAPESP grant 2019/08783-0 (GML)
FAPESP grant 2019/09813-0 (MGV)
FAPESP grant 2020/04608-7 (DROR)
FAPESP-NERC grant 18/50080-4 (GC)
FAPITEC (CSL & ASR)
FAPITEC/SE/FUNTEC grant 01/2011 (MAP)
FCT - Portuguese Foundation for Science and Technology grant UIDB/04033/2020 (JLPCL)
FONDECYT grant BM-INC.INV 039-2019 (MEF)
Fulbright Fellowship (BJE)
German Academic Exchange Service (DAAD) (MR)
German Research Council (MM)
HELVETAS Swiss Intercooperation (MEF)
IAI-SGP-CRA grant 2047 (JVD)
IFS grant D/5466-1 (JHS)
IFS grant D/5466-1 (JN)
Inter-American Institute for Global Change Research IAI (FAR)
ITTO Fellowship Award grant 046/12S (EJRR)
Lamont Climate Center (BMB)
Mahidol University grant FRB660042/0185 (NP)
María Zambrano postdoctoral research program MZ2021 (RaAS)
Minciencias grant 1118-714-51372 (IRNM)
Ministerio Ciencia grant TED2021-129770B-C22 (RSS)
National Geographic Global Exploration Fund grant GEFNE80-13 (IR)
National Natural Science Foundation of China grant 31870591 (PF)
National Research Council of Thailand (NRCT) grant N42A660392 (PT)
NSF grant AGS-1501321 (DGS)
NSF (BMB)
NSF CREST grant 0833211 (KSF)
NSF grant IBN-9801287 (AJL)
NSF grant AGS-1501321 (GAP)
NSF grant AGS-2102888 (JM)
NSF grant AGS-2102938 (GLH)
NSF grant GER 9553623 (BJE)
NSF Postdoctoral Fellowship (BJE)
NSF-FAPESP PIRE grant 2017/50085-3 (CF & MTF)
NSF-FAPESP PIRE grant 2019/27110-7 (CF)

NUFFIC (JHS & JN)
NUFFIC-NICHE . (EM)
PIRE-CREATE grant 2017/50085-3 (MGV)
PROCAD-AM grant 88887.625854/2021-00 (BH)
Proyectos de generacion de conocimiento grant PID2021-123675OB-C44 (RSS)
Schlumberger Foundation (JHS & JN)
Short-term fellowship from the Smithsonian Tropical Research Institute (RaAS)
Sigma Xi (AJL)
Spanish Agency for International Development Cooperation (KPV)
Thailand Science Research and Innovation Fund Chulalongkorn University (PT)
The Copperbelt University (JHS & JN)
The National Institute of Science and Technology in Plant Physiology under Stress Conditions grant 406455/2022-8 (FAL)
UK NERC grant NE/K01353X/1 (EG)
UKRI grant EP/X025098/1 (NJL)
UKRI grant NE/B501504 (NJL)
UNAM-PAPIIT grant IN110223 (LVS)
Universidad Autónoma Agraria Antonio Narro (ECO)
World Wildlife Fund (WWF) (KPV)
Xunta de Galicia grant ED431C 2023/19 (GPL)
Xunta de Galicia grant ED481D 2023/012 (GPL)

Author contributions:

Conceptualization: PAZ, FB, PG, MR, and VT

Data contribution: all co-authors except FB

Data analysis: PAZ, FB, MR and PG.

Writing – original draft: PAZ and FB, with important contributions from VT, MR, and PG

Writing – review & editing: all co-authors

Competing interests: Authors declare that they have no competing interests.

Data and materials availability: All tree growth anomalies during and after drought years from the 483 tree-ring chronologies included in the study are provided as a supplementary Data S1. All 483 chronologies (from 1930 onwards) are available publicly available in DataDryad (*54*). Raw tree-ring width measurements all 483 chronologies are publicly available (free of charge and for all research purposes) on the International Tree-Ring Data Bank (ITRDB) (*55*). Links to the raw data of all 483 chronologies available on the ITRDB are included in DataS1.csv (supplementary file) and in the metadata_FINAL.csv on DataDryad (*54*). All code to build chronologies from raw tree-ring data,

process climate data, conduct superposed epoch analyses, statistical analyses and production of figures is deposited on DataDryad (*54*).

Supplementary Materials:

Materials and Methods

Figs. S1 to S18

Table S1

References (55-75)

Data S1

Figure legends

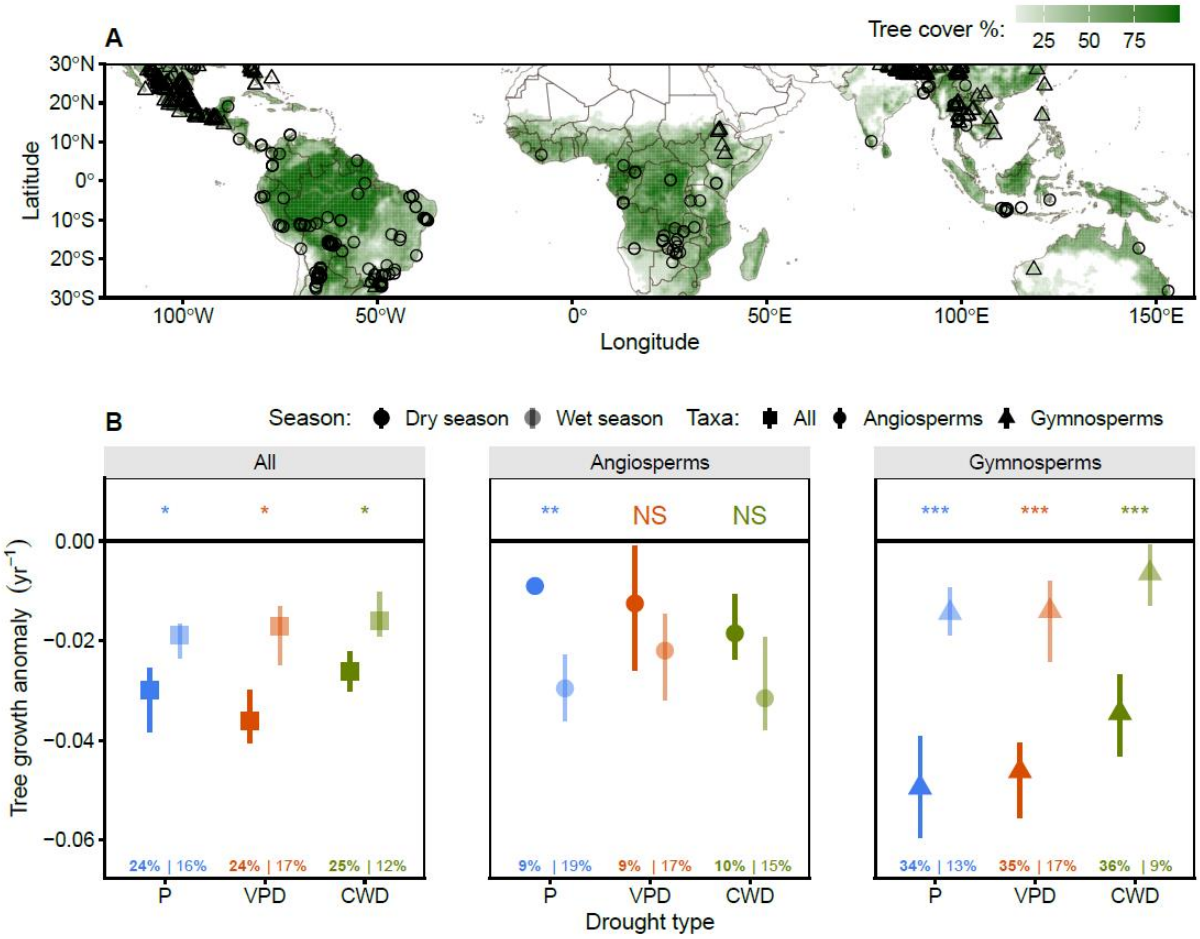

Fig. 1. Pantropical growth anomalies during drought years obtained from a tree-ring network. (**A**) Geographical distribution of 483 tropical tree-ring width chronologies from gymnosperms (n=273, triangles) and angiosperms (n=210, circles). The background color is tree cover percentage (>10%). (**B**) Pantropical median anomalies of annual tree growth (whiskers: bootstrapped 95% confidence intervals) during the 10% years with the lowest precipitation (P), highest vapor pressure deficit (VPD), or highest climatic water deficit (CWD). Results are shown for droughts occurring during the dry (filled symbols, bold text) and wet seasons (transparent symbols, normal text), and for angiosperms and gymnosperms combined ('All') or separately. Results of weighted Mann Whitney U tests between seasons are shown (NS: p >0.05; *: p <0.05; **: p <0.01; ***: p <0.001). No significant differences in growth anomalies were found between drought types for any combination of species groups and season (Kruskal Wallis tests, p >0.05). Percentage values represent the proportion of significant negative anomalies in SEA analyses (p<0.05). Sample size per symbol is in Table S1B.

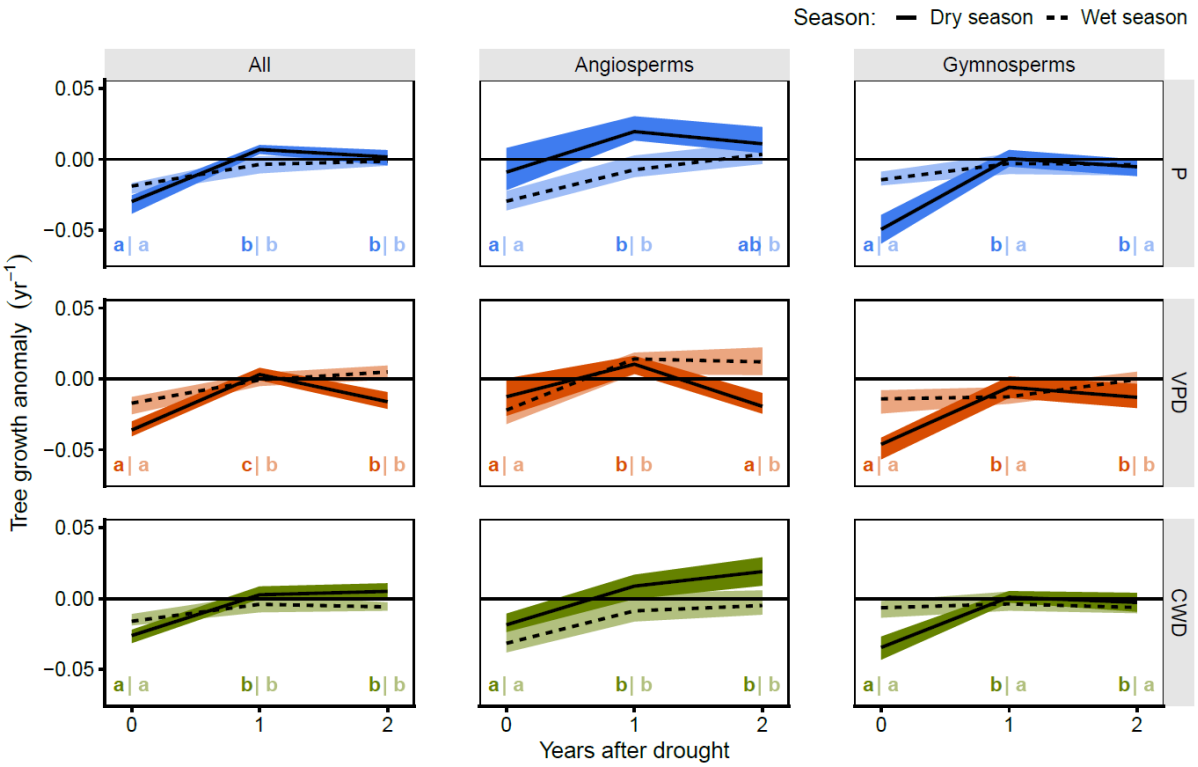

Fig. 2. Drought effects on pantropical tree growth are short-lived. Growth anomalies during and following years with low precipitation (P), high vapor pressure deficit (VPD), or high climatic water deficits (CWD). Responses are shown for dry- and wet-season droughts, and for angiosperms and gymnosperms combined ('All') or separately. Bands show bootstrapped 95% confidence intervals of medians. Different letters indicate a significant difference between years (Mann Whitney U tests; $p<0.05$) per season (**dry** | wet). Sample size per line is in Table S1B.

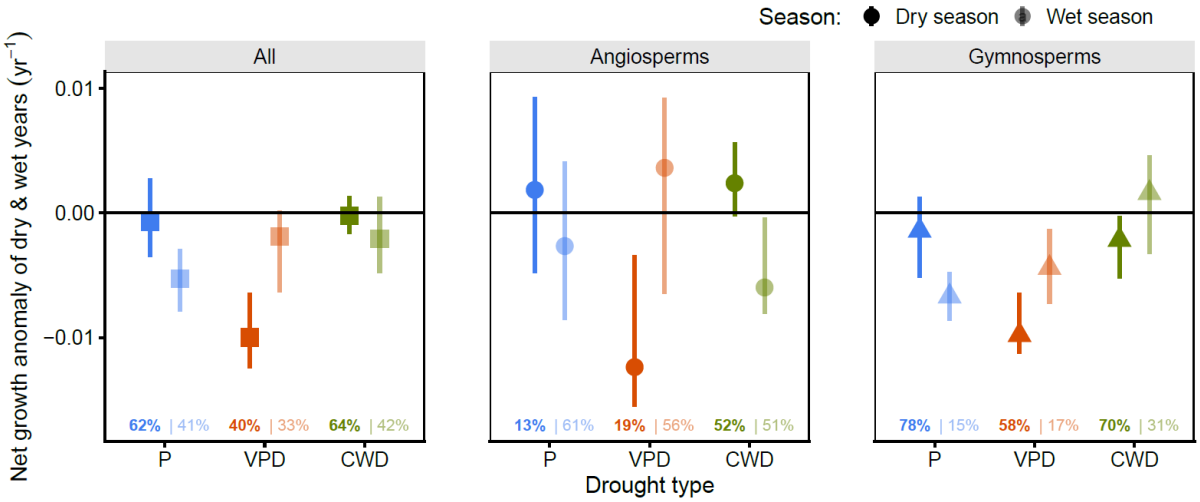

Fig. 3. Wet extremes partially mitigate drought effects on tropical tree growth. Pantropical medians (and bootstrapped confidence intervals) of the net growth anomaly of dry and wet extreme years. Results are shown for extremes occurring in the dry or wet seasons and for angiosperms and gymnosperms combined ('All') or separately. Droughts (and wet extremes) were identified as the 10% years with the lowest (highest) precipitation, highest (lowest) vapor pressure deficit (VPD), or highest (lowest) climatic water deficit (CWD). The net anomaly was calculated as the average of the anomalies of the dry and wet extreme years. Percentages denote the growth loss during drought years that is mitigated during wet extremes per season (**dry** | wet). Sample size per symbol is in Table S1B.

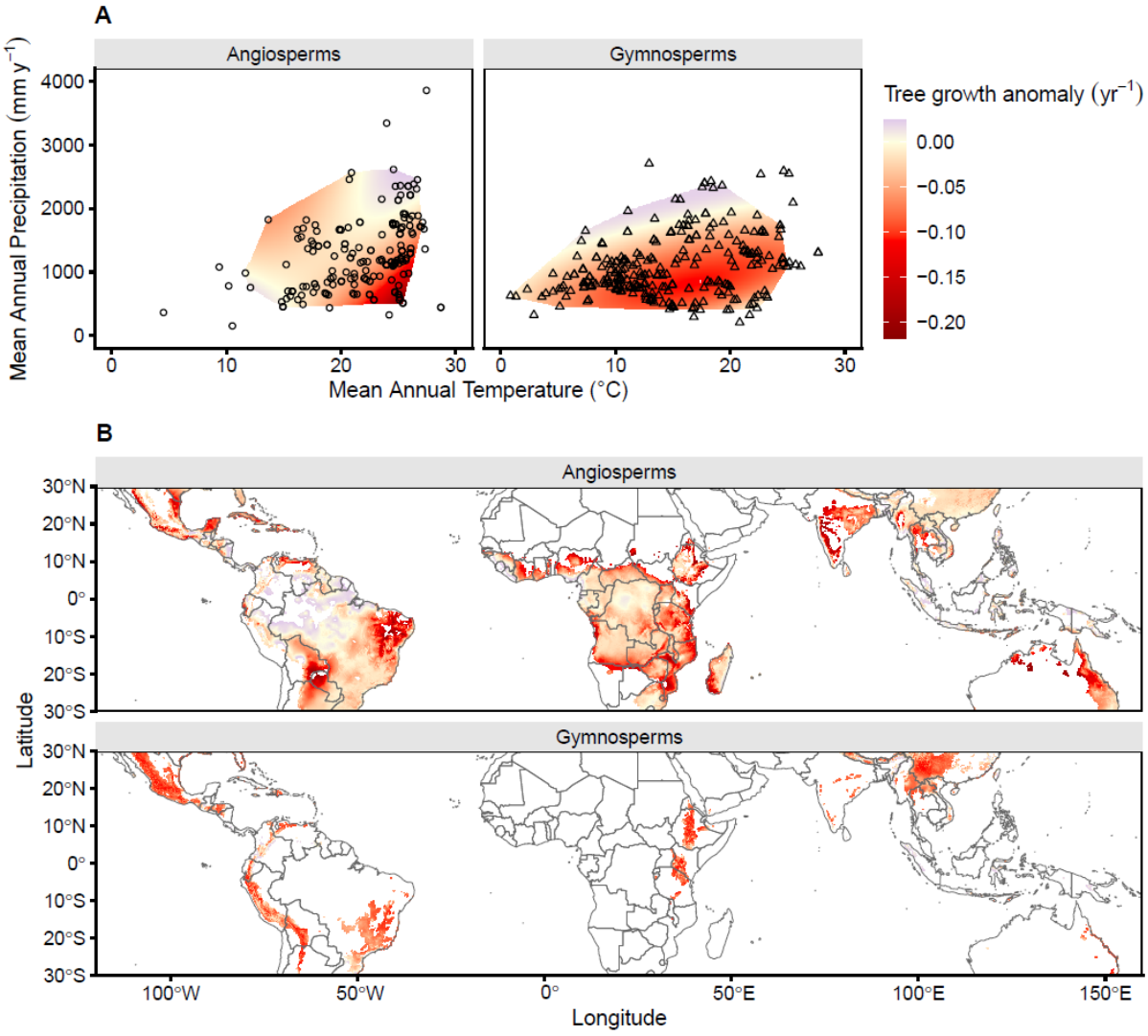

Fig. 4. Climatic and spatial distribution of drought-induced anomalies of tropical tree growth. (**A**) Growth anomalies during years with low precipitation during the wet (angiosperms, n=210) and dry seasons (gymnosperms, n=273) interpolated across climate space. The interpolated climate space was restricted to 95% of the climatic ranges of precipitation and temperature. (**B**) Projections of the interpolated values from (A) into geographic space. The geographic distribution of gymnosperms was restricted to elevations >700 m above sea level (i.e., the 10th percentile of their elevational distribution). For Africa, the gymnosperm distribution was further restricted by a species distribution model of the only African gymnosperm in our network (*Juniperus procera*).

Supplementary Materials for

'Pantropical tree growth resilience to drought'

Authors: Pieter A. ZUIDEMA, Peter GROENENDIJK, Mizanur RAHMAN, Valerie TROUET, Abrham ABIYU, Rodolfo ACUÑA-SOTO, Eduardo ADENESKY-FILHO, Raquel ALFARO-SÁNCHEZ, Claudio Roberto ANHOLETTO JUNIOR, José Roberto Vieira ARAGÃO, Gabriel ASSIS-PEREIRA, Claudia C. ASTUDILLO-SÁNCHEZ, Ana Carolina BARBOSA, Giovanna BATTIPAGLIA, Hans BEECKMAN, Paulo Cesar BOTOSSO, Nils BOURLAND, Achim BRÄUNING, Roel BRIENEN, Matthew BROOKHOUSE, Supaporn BUAJAN, Brendan M. BUCKLEY, J. Julio CAMARERO, Artemio CARRILLO-PARRA, Gregório CECCANTINI, Librado R. CENTENO-ERGUERA, Julián CERANO-PAREDES, Wirong CHANTHORN, Ya-Jun CHEN, Bruno Barçante Ladvocat CINTRA, Eladio Heriberto CORNEJO-OVIEDO, Otoniel CORTÉS-CORTÉS, Clayane Matos COSTA, Camille COURALET, Doris Bianca CRISPÍN-DE-LA-CRUZ, Rosanne D'ARRIGO, Diego A. DAVID, Maaike DE RIDDER, Jorge Ignacio DEL VALLE, Mário DOBNER JR, Jean-Louis DOUCET, Oliver DÜNISCH, Brian J. ENQUIST, Karin ESEMANN-QUADROS, Gerardo ESQUIVEL-ARRIAGA, Ze-Xin FAN, Adeline FAYOLLE, Tatiele Anete Bergamo FENILLI, M. Eugenia FERRERO, Esther FICHTLER, Patrick M. FINNEGAN, Claudia FONTANA, Kainana S. FRANCISCO, Pei-Li FU, Franklin GALVÃO, Aster GEBREKIRSTOS, Jorge A. GIRALDO, Emanuel GLOOR, Milena GODOY-VEIGA, Daniela GRANATO-SOUZA, Anthony GUERRA, Kristof HANECA, Grant Logan HARLEY, Ingo HEINRICH, Gerhard HELLE, Bruna HORNINK, Wannes HUBAU, Janet G. INGA, Mahmuda ISLAM, Yu-Mei JIANG, Mark KAIB, Zakia Hassan KHAMISI, Marcin KOPROWSKI, Eva LAYME, A. Joshua LEFFLER, Gauthier LIGOT, Claudio Sergio LISI, Neil J. LOADER, Francisco De Almeida LOBO, Giuliano Maselli LOCOSSELLI, Tomaz LONGHI-SANTOS, Lidio LOPEZ, María I. LÓPEZ-HERNÁNDEZ, José Luís Penetra Cerveira LOUSADA, Rubén D. MANZANEDO, Amanda K. MARCON, Justin T. MAXWELL, Omar N. MENDOZA-VILLA, Ítallo Romany Nunes MENEZES, Mulugeta MOKRIA, Valdinez Ribeiro MONTÓIA, Eddy MOORS, Miyer MORENO, Miguel Angel MUÑIZ-CASTRO, Cristina NABAIS, Anuttara NATHALANG, Justine NGOMA, Francisco De Carvalho NOGUEIRA

JR., Juliano Morales OLIVEIRA, Gabriela Morais OLMEDO, Daigard Ricardo ORTEGA-RODRIGUEZ, Carmen Eugenia Rodríguez ORTÍZ, Mariana Alves PAGOTTO, Shankar PANTHI, Kathelyn PAREDES-VILLANUEVA, Gonzalo PÉREZ-DE-LIS, Laura Patricia PONCE CALDERÓN, Leif Armando PORTAL-CAHUANA, Darwin Alexander PUCHA-COFREP, Nathsuda PUMIJUMNONG, Paulo QUADRI, Jorge Andrés RAMÍREZ, Edilson Jimmy REQUENA-ROJAS, Judith REYES-FLORES, Adauto De Souza RIBEIRO, Iain ROBERTSON, Fidel Alejandro ROIG, José Guilherme ROQUETTE, Ernesto Alonso RUBIO-CAMACHO, Raúl SÁNCHEZ-SALGUERO, Ute SASS-KLAASSEN, Jochen SCHÖNGART, Marcelo Callegari SCIPIONI, Paul R. SHEPPARD, Lucas C.R. SILVA, Franziska SLOTTA, Leroy SORIA-DÍAZ, Luciana K.V.S. SOUSA, James H. SPEER, Matthew D. THERRELL, Ginette TICSE-OTAROLA, Mario TOMAZELLO-FILHO, Max C.A. TORBENSON, Pantana TOR-NGERN, Ramzi TOUCHAN, Jan VAN DEN BULCKE, Lorenzo VÁZQUEZ-SELEM, Adín H. VELÁZQUEZ-PÉREZ, Alejandro VENEGAS-GONZÁLEZ, Ricardo VILLALBA, Jose VILLANUEVA-DIAZ, Mart VLAM, George VOURLITIS, Christian WEHENKEL, Tommy WILS, Erika S. ZAVALETA, Eshetu Asfaw ZEWDU, Yong-Jiang ZHANG, Zhe-Kun ZHOU, Flurin BABST

Corresponding author: Pieter A. Zuidema, pieter.zuidema@wur.nl

This file includes:

Materials and Methods

Figs. S1 to S18

Table S1

Dataset S1

Materials and Methods

Tree-ring network.

We used tree-ring data from naturally regenerating tree populations in tropical and subtropical vegetation (30°N to 30°S; fig S1A-C). We compiled raw ring-width data from the ITRDB (International Tree-Ring Databank, https://www.ncdc.noaa.gov/data-access/paleoclimatology-data/datasets/tree-ring) (339 chronologies) and contributing authors (144 chronologies). Raw ring-width data for 98 out of the 339 chronologies available on the ITRDB had been uploaded as part of an earlier publication from the Tropical Tree-ring Network network (*17, 18*) (see www.tropicaltreeringnetwork.org).

We selected chronologies that extended for at least 30 years beyond 1930 (our quality-based cut-off year for climate data) to obtain a minimum of three drought years (taking the 10% driest years). After selection, our dataset contained 483 chronologies, representing >10,000 trees, 163 species, 33 plant families and an average chronology length (since 1930) of 56 years. Local field data on vegetation structure, soil type, sampling strategy and tree-level metrics (diameter, height, location) were unfortunately unavailable. While this limits interpretation of local drought responses, it does not hamper the pantropical-level analyses we aimed for.

Within the network, proportions of gymnosperms (55%) and angiosperms (45%) are similar. Tropical gymnosperms typically occur at high elevation: on average 2330 m a.s.l. within the network, as reflected in the respective climate space (fig S1D). Leaf habit differs markedly between groups: 74% of angiosperm chronologies belongs to deciduous species, whereas this percentage is 11% for gymnosperm chronologies. Local species richness also differs, with gymnosperm sites containing an estimated 9 species per hectare compared to 36 for angiosperm sites (species richness estimates extracted from Ref (*56*), fig. S1E). To assess tree density at our sites and mask out areas with <10% tree density, we obtained MODIS-derived tree-cover percentages for all sites ('Percent_Tree_Cover', MOD44B, version 6; https://lpdaac.usgs.gov/products/mod44bv006/).

Chronology building.

To ensure that drought effects on radial tree growth are comparable across sites, we constructed single-species chronologies from raw ring-width series by applying a single detrending procedure. To assess effects of droughts occurring during a single year (i.e., excluding extended droughts), we chose to apply a flexible detrending of the raw ring-width series that removes low-frequency (decadal to centennial) variation and retains the high-frequency (annual) variation of interest. After testing spline detrending with various degrees of flexibility, we chose to use a spline with a 50% frequency cut-off at 20 years for the main analyses. We tested whether drought effects are sensitive to the choice of spline flexibility by repeating our analyses with 10 and 30-year splines. Next, we developed mean chronologies of ring-width index (RWI) from the detrended series using a bi-weight robust mean and truncated them in 1930. For all tree-ring series from the Southern Hemisphere (SH), the calendar year assigned to the ring was that during which ring formation starts ('Schulman convention'). The only SH region where this convention was not applied is the Brazilian Caatinga, where the growing season coincides with the calendar year (*57*). Detrending and chronology building was conducted in R (*58*) using the dplR package (*59*).

Climate data, season definition, and identifying droughts.

To characterize mean site climate, we used the high-resolution (~ 1 km) gridded climate data from Worldclim version 2 (*60*) to obtain 30-year (1970-2000) mean annual temperature (MAT, in °C) and precipitation (MAP, in mm) and mean monthly precipitation. We used mean monthly precipitation (30-year average) to define seasons for each site: the wet season consisted of all months with >100 mm average precipitation; the dry season was defined as all months with less than 100 mm precipitation, preceding the wet season. We chose this dry-season timing because climate sensitivity of

annual stem growth of tropical trees was found to be larger for the dry months before the wet season than those after the wet season (*17*).

To identify drought years, we used monthly time series from the spatially coarser (0.5°) gridded climate data from the Climate Research Unit Time Series (CRU TS4.05) (*61*). We used CRU data time series starting in 1930, seeking a compromise between extending the time series to include more drought years and the decreasing quality of gridded climate data back in time, particularly in remote tropical regions. We used CRU data to identify three types of droughts: those defined by low precipitation (P), high vapor pressure deficit (VPD), or high climatic water deficit (CWD, expressed as positive values). We selected these drought metrics because (1) they represent different types of droughts (i.e., soil water availability vs atmospheric water demand), (2) CWD droughts may represent additive effects of soil and atmospheric droughts, and (3) they will likely shift at a different pace and pattern under continued climate change. We specifically included P droughts as these are directly based on meteorological measurements and require fewer assumptions and additional data sources compared to CWD, VPD. We did not take the possibly modifying effect of rising atmospheric CO_2 on drought responses into account because the periods covered differ strongly between chronologies and reported direct CO_2 effects on tree growth are small (*62, 63*).

VPD was calculated from CRU products as saturated minus actual vapor pressure. The former was derived from monthly mean temperature, the latter is available as a standard CRU product. CWD was calculated as the sum of the climatic water balance (P-PET) of all months during the (wet or dry) season when potential evapotranspiration (PET in mm, available as a CRU product) exceeded precipitation. Thus, our approach uses the water balance to obtain monthly deficits, which are summed over the season to obtain the seasonal deficit. Time series for each of these drought metrics were obtained for dry and wet seasons separately, and detrended with the same flexible spline as the tree-ring data (i.e., 50% frequency cut-off at 20 years) to remove climatic trends and low-frequency variation (*64*). Next, we identified extreme years at each site for all six combinations of drought types and seasons for the timespan covered by chronologies since 1930. To do so, we selected the 10% years with the lowest seasonal precipitation, highest seasonal VPD, or highest seasonal CWD. We evaluated trends (since 1930) in the frequency and intensity of drought years (number of SD away from the long-term mean value of the climate variable); and we calculated the frequency of droughts spanning two or more years (i.e., the drought length).

To evaluate the robustness of our results towards the threshold for selecting extremes, we repeated our SEA analyses for the 5% most extreme years (for 425 chronologies with >60 years of data since 1930) and for those sites for which the mean precipitation, VPD, or CWD of the extreme years exceeded >1.5 SD of the time series. In addition, we also evaluated the effects of droughts lasting for two consecutive years. To do so, we selected the year pairs (e.g., 1958-1959, or 1982-1983) that exhibit the 10% lowest P (over any 2-year period), highest VPD, or highest CWD.

To verify the robustness of our results to the source of climate data, we conducted analyses of drought effects using two newer climate products which have a higher spatial resolution but cover a shorter period. (1) TerraClimate (TC) (*65*) is based on CRU, but has a higher spatial resolution and a considerably smaller temporal coverage (from 1958 onwards). We extracted monthly values for our study sites of precipitation (ppt), VPD (vpd)), and Potential evapotranspiration (pet),) from which CWD was derived as P-PET. (2) ERA5 (*66*) also has a higher spatial resolution than CRU, extends back in time to 1940, but is a re-analysis product and thus less directly based on climate station data. We extracted monthly values of Precipitation, VPD and PET, and then calculated CWD as P-PET. Despite differences in climate correlations and drought years selected (fig. S10), growth anomalies differed in only 2 out of 36 tested comparisons (fig. S11).

Drought effects.

We evaluated drought effects on tree growth during extreme years and the following two years using Superposed Epoch Analysis (SEA). SEA is used in tree-ring analysis to quantify and test the significance of ring-width anomalies during rare events, including climate extremes (*21, 22, 67*) and volcanic eruptions (*24*). We used the "sea()" function from the dplR package (*59*), which calculates

mean RWI values during a specified range of years around events, generates 1000 bootstrapped distributions of RWI values from the chronology (with a sample size equal to the number of event years, and a minimum of 3 in this study), compares the mean of the 'event RWI' values with the randomly generated RWI distributions and returns a the probability that 'event RWI' values differ significantly from 'normal' years ($p<0.05$).

We modified the SEA function in two ways. First, we excluded years prior to event years, because pre-drought effects on growth are not expected. Second, we modified the function such that it does not use any of the event years (nor the two following years) to generate bootstrapped RWI distributions of normal years. This was done to prevent the generated normal RWI distribution from containing event years to which they are compared. Test runs showed that the first modification had little effect on the SEA results, but the second one caused a slight increase in the probability of significant differences.

We also performed SEA analyses for all individual tree-ring series to provide a first indication of how common the significant growth declines are within the studied populations. We used the same procedure as for chronology-level analyses, selecting only those series that covered at least three droughts. We then registered which individual series showed a significant negative growth anomaly during the drought years and obtained the percentage of significant series per chronology. To verify whether series-level growth declines are more common when chronology-level growth declines are larger, we associated these metrics (fig. S8). We also calculated the median percentage significant series per drought type and season. The series-level results need to be interpreted with caution for various reasons: (i) Ring-width series do not correspond to individual trees and can therefore not be interpreted as tree-level responses. (ii) Ring-width series may have been excluded during chronology construction because of poor cross dating. This may result both from low responsiveness to climatic fluctuations as well as from very strong responses leading to missing rings. (iii) Variation in the significance percentages across sites can be caused by differences in sampling strategy, including the specific size distributions sampled, the genetic makeup of the sampled individuals, the extent to which local environmental variability (microsites) was included in the sampled population and the degree to which temporal growth variation of sampled trees was influenced by forest dynamics (canopy disturbances, biotic stressors).

To verify whether drought-induced anomalies in RWI from SEA analyses can be interpreted as proportional shifts in ring width, we evaluated the effect of synthetic reductions of raw ring-width on RWI. For each chronology, we reduced raw ring width of all ring-width series by 10% for several artificial 'drought years' corresponding to 10% of the duration (in years) of each series. The set of artificial 'drought years' was randomly selected for each chronology, but fixed for all tree-ring series within a chronology. We then detrended the modified ring-width series and constructed chronologies of RWI. Per chronology we checked the RWI anomaly for the artificial 'drought years' and compared that to the induced growth reduction. We repeated this procedure for synthetic growth reductions of 20 and 30%, thus covering the range of site-level RWI changes during individual drought years. The resulting distributions of RWI anomalies (averaged per chronology) during artificial drought years were narrow, with medians very close to the artificially applied growth reduction (fig. S3). Median RWI anomalies were approximately 10% smaller than the implemented growth reduction (i.e., RWI was reduced by 9, 18 and 27% instead of the tested 10, 20 and 30%), suggesting that growth anomalies from SEA analysis slightly underestimate actual drought effects on stem radial growth.

Weighted pantropical medians and their confidence intervals.

To account for the higher abundance of tree-ring studies at high elevation and in arid climates (fig. S2), we weighted sites by climatic conditions. First, we compared probability density functions of the drought metrics (precipitation, VPD, and CWD) for our tree-ring sites with those for all forested tropical land area (tree cover >10%). Both sets of density functions were re-scaled from 0 (climate value does not occur) to 1 (climate value is most common) by dividing by their respective maximum. Next, we used the scaled density value of forested land area for a particular drought metric of a site as

weight when calculating pantropical median growth anomalies for that drought metric, and also in our interpolation and path analyses.

To estimate the sensitivity of pantropical weighted medians of growth anomalies to the particular composition of the tree-ring network, we calculated bootstrapped 95% confidence intervals (CI). We obtained CI from the distribution of 1000 calculations of the weighted median based on random draws of 75% of the sites in the network. This was done for all pantropical medians presented.

Wet extremes.

To put results of our drought analysis into perspective, we also performed SEA analyses for the 10% wettest years, selecting years with highest seasonal P, lowest VPD, or lowest CWD. This analysis is the same as that for drought years, with the only difference that the 10% wettest years are selected as event years and their RWI anomaly is compared to normal years in an SEA analysis, using the modified SEA function (see above under 'Drought effects'). Combining results from dry and wet extremes, we then calculated two metrics per site. (i) The average growth anomaly was calculated by summing the anomalies of dry and wet extreme years and dividing this by 2 (to obtain an annual anomaly). (ii) The percentage of negative growth anomalies during drought years that is mitigated by responses during wet extremes was calculated by dividing the (mostly positive) growth anomaly during wet extremes by the absolute value of the growth reduction during drought years for each chronology.

Path analysis.

Previous tree-ring studies have shown that drought-induced growth anomalies tend to be stronger for chronologies with higher first-order temporal autocorrelation (*22*). To assess the magnitude of this effect, we conducted path analyses that separate the direct effects of climate (MAP, MAT and interannual variability of P, VPD and CWD) on growth anomalies during droughts from the indirect effects through temporal autocorrelation. We verified whether tree cover (MODIS) explained growth anomalies but left this out of the final path analyses because it was significant in only one of out 12 combinations of taxa, seasons and drought types. We also added wood density (from *68*) to the model as an indicator of drought tolerance. For each chronology, we obtained first-order autocorrelation using the function *ar1* in the dplR package (*59*). Path analysis was conducted for gymnosperms and angiosperms separately and for year 0 when drought effects were strongest. We scaled climate variables and wood density, and weighted sites by climatic representativeness (see above under 'Weighted pantropical medians and their confidence intervals.'). Path analysis was conducted using the *lavaan* package in R (*69*).

Interpolation in climate space and mapping.

To assess geographic variation in RWI anomalies during droughts, we generalized our site-level observations using a spatial interpolation approach. We did so for angiosperms and gymnosperms separately. Doing the interpolation directly in geographic space was not feasible due to the heterogeneous site distribution of the sites. Therefore, we performed the spatial interpolation in climatic space (i.e., MAT and MAP space) where the coverage of our network is much better (fig. S14). To reduce possible edge effects in poorly represented climates, we restricted this climatic space to 95% of the MAT and MAP range that is covered by the sites in our tree-ring network. Following a previous tree-ring study (*70*), we used a third-order polynomial trend surface interpolation to project site-specific growth anomalies into climatic space. Interpolation was conducted only for year 0, when drought effects were strongest. Uncertainty in the spatial interpolation was assessed using a Monte Carlo-type resampling, in which 25% of the network was randomly excluded during each of 1000 draws (with replacement) and a trend surface was obtained. The standard deviation of the resulting 1000 trend surfaces was then used as a spatially resolved uncertainty metric. Uncertainties were

overall low (fig. S15), but largest at the cool-humid edges of the climate space, where coverage of our network is sparse.

Knowing the MAT and MAP of each grid cell across the wooded (>10% tree cover) tropical land area, we then sampled the trend surfaces and produced geographic maps of growth anomalies (and their uncertainty; fig. S17) during drought. This procedure was performed for the drought types with the strongest impacts and for interpolation models with the highest R^2: wet-season precipitation for angiosperms and dry-season precipitation for gymnosperms. For the gymnosperm map, we additionally masked out all elevations <700 m a.s.l. (representing the 10^{th} percentile of their altitudinal distribution in the network). For Africa, we further limited the map using a species distribution model of the only African gymnosperm species in the network (*Juniperus procera*). The species distribution model (Maxent) was based on occurrence data from the Global Biodiversity Information Facility (GBIF) extracted using the rgbif package (*71*) and Worldclim2 climate data.

Estimating additional mortality risks from growth reductions.

Strong drought-induced growth reductions may be associated with tree stress and may thus increase mortality risk, often after some delay (*72*). Tree-ring studies found indirect evidence for this: the growth rates and growth resilience to droughts of dead trees were lower than those of alive trees (*73, 74*). Yet, such comparative studies cannot be used to estimate additional mortality risks following droughts and are not available for tropical trees. Ideally, estimates of additional mortality risk are based on monitoring of tree growth and mortality during and following droughts. Studies doing so for droughts and at annual resolution are unavailable in the tropics, but more generic associations between mortality risk and growth anomalies at longer time intervals have been analyzed in field studies across 10 tropical forest sites (*49*, *75*). We made use of one such study (*49*) to provide a first and approximate estimate of the order of magnitude of tree mortality associated with the drought-induced tree growth reductions found in our study. The field study we used was conducted on >1100 tree species in 10 large plots (20-50 ha) in lowland tropical forests (*49*). The climate space covered by these plots overlaps notably with that of lowland angiosperm chronologies in our study (Fig S18A). These field studies established empirical relationships between mortality risks during one census interval (of ~5 years) and stem growth anomalies in the previous interval. We recognize that growth anomalies from this study may have resulted from other causes than droughts (e.g., pests, diseases, canopy closure or branch loss) and that the longer time interval over which anomalies were calculated average out strong growth reductions during anomalous years. We therefore cautiously interpret our estimates of additional drought-induced mortality, considering them merely an estimate of the order of magnitude.

Specifically, we applied the following equation and coefficients from ref (*49*):

$$\text{logit}(p) = \beta_0 + \beta_1 * \ln(D) + \beta_2 * g^{0.45}$$

in which p is mortality probability (per 5 years), D is diameter (set to 200 mm, the estimated diameter of sampled trees in our network), g is diameter growth rate (set to 2 mm per year as baseline growth rate), β_0 is the intercept (set to -1.78, which is the average of the 10 plots from Supplementary Figure 2 in (*49*)), β_1 is the coefficient defining the size-mortality relationship (not provided in ref (*49*)), and β_2 is the coefficient defining the growth-mortality relationship (set to -2.04, which is the average of the 10 plots from Supplementary Figure 2 in (*49*)). Because the β_2 coefficient determines the association between growth decline and additional mortality, we also performed an analysis in which β_2 was sampled from a distribution of site-specific values (SD=0.802). To get an estimate for the unknown coefficient β_1 we set background ('normal') mortality (annualized p) to 1% annually, taking the lower estimate from the larger ForestGEO plot network (1-4%) (*76*) to reflect the larger size of trees sampled for tree ring analysis. The resulting β_1 was 0.3. To obtain estimates of drought-induced additional mortality risks for each of the drought types and seasons, we (i) selected chronologies with negative growth anomalies during drought years (459 chronologies), (ii) selected chronologies from angiosperm species at lowland sites (<1000 m a.s.l.), because the studied tropical forest plots are dominated by angiosperms (158 chronologies), (iii) multiplied g in the above equation by (1- growth

anomaly) for each chronology (growth anomaly based on 10% drought years) to obtain an estimate of *p*, which was annualized and from which the baseline mortality (1%) was subtracted to get an annual additional mortality risk, (iv) conducted this analysis for 1000 bootstrapped subsets of 75% of sites (as above under 'Weighted pantropical medians and their confidence intervals.') with a fixed β_2 value (the across-site mean of -2.04), (v) re-ran these analyses for 1000 bootstrapped subsets with β_2 values sampled from its distribution (mean=-2.04, SD=0.802), (vi) calculated weighted medians for each bootstrap run, (vii) calculated bootstrapped 95% confidence intervals, and (viii) repeated this for growth anomalies found for 5% drought years.

Figs. S1 to S18

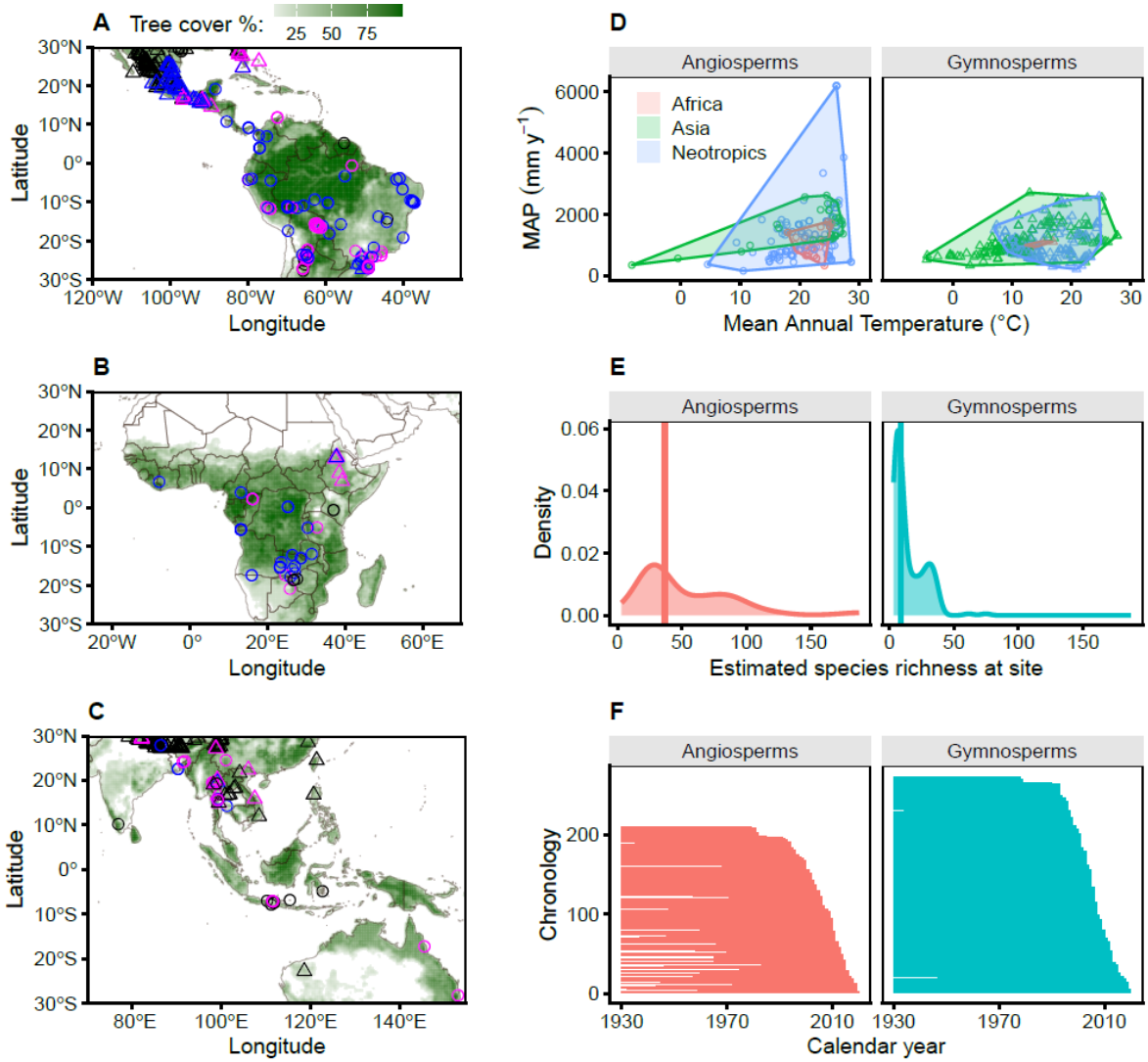

Fig. S1. Distributions and characteristics of tropical tree-ring chronologies included in this study. (A-C) Geographical distribution of chronologies in the Neotropics (**A**, n=280), Africa (**B**, n=42) and Asia and Australia (**C**, n=161), specifying the data source and major taxonomic clade (circles: Angiosperms, triangles: Gymnosperms). Sources and availability of raw data: black symbols, available in the ITRDB (International Tree-Ring Databank) before 2022 (241 chronologies); blue symbols, added to ITRDB in 2022 as part of an earlier study (*17*) (98 chronologies); purple symbols, added to the ITRDB for the current study (144 chronologies). Background color is tree cover percentage (minimum of 10%) from MODIS. **(D)** Continental distributions of study sites in climate space. Median values of mean annual precipitation (MAP) and temperature differ significantly between continents (Kruskal Wallis test, $p<0.05$). **(E)** Distributions of the estimated local tree species richness from Ref (*56*), with vertical line indicating the median. **(F)** Temporal coverage of chronologies.

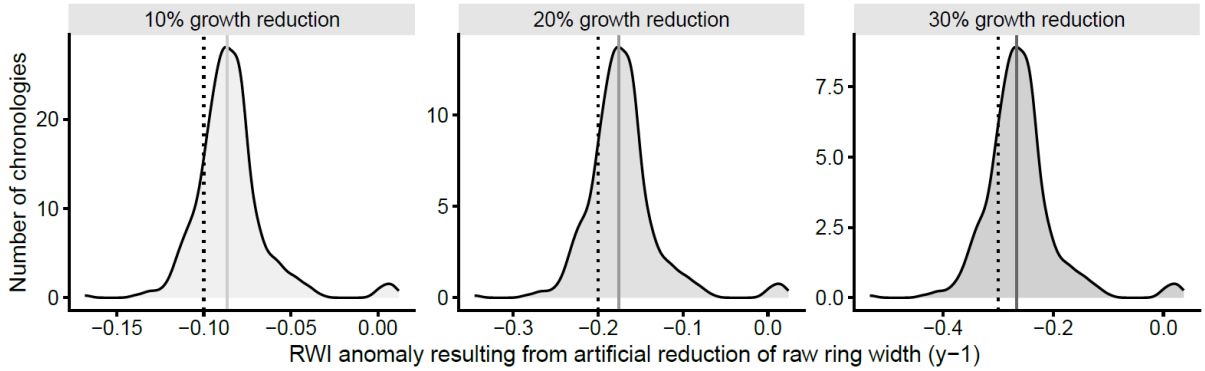

Fig. S2. Anomalies in Ring-Width Index (RWI) can be interpreted as proportional changes in ring width. Shown are distributions of RWI anomalies resulting from artificial implementation of growth reductions in raw ring-width data by 10, 20 or 30% to the entire tree-ring network (n=483 chronologies). For these three growth reduction scenarios, RWI distributions are narrow, with median values (solid lines) close to that of the implemented artificial growth reduction (dotted lines). Median RWI anomalies underestimate artificial changes by approximately 10%. This underestimation was not accounted for in the reported growth anomalies.

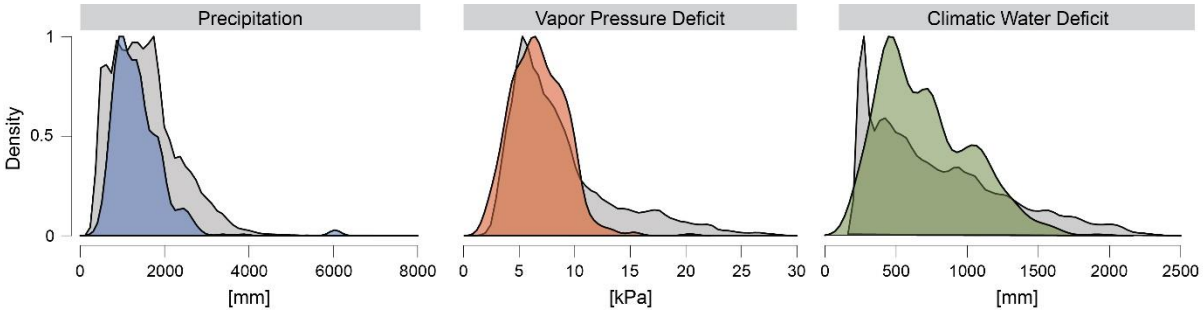

Fig. S3. Climatic representativeness of the tropical tree-ring network. Shown is relative density (scaled to a maximum of 1) of the chronology sites (color-coded) and tropical land area with woody vegetation (grey, cover >10% in the MODIS land-cover product), for each of the three drought types used in the analysis. The land area density is used as a weighting variable to calculate medians (and other percentiles) and in all statistical analyses.

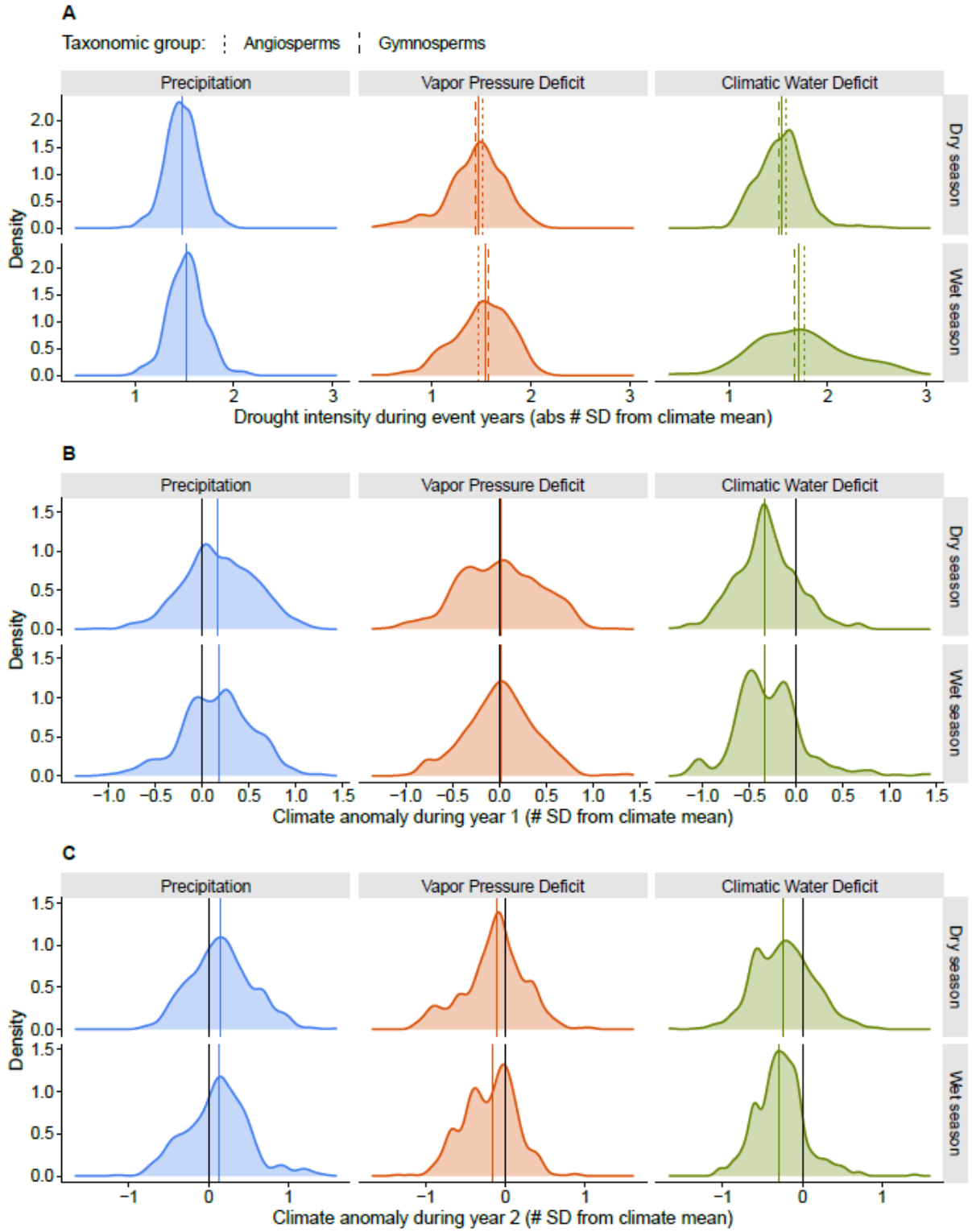

Fig. S4. Drought intensity during and after extreme years. (A) Distributions of drought intensities during the 10% most extreme years in terms of precipitation, VPD and CWD. Drought intensity is expressed as a climate anomaly: the number of standard deviations (SD) away from the mean climate. Vertical lines are median values for all (solid), angiosperm (dotted) and gymnosperm (dashed) chronologies. **(B-C)** Climate anomalies during the first (B) and second (C) post-drought year. Climate anomalies are calculated as in A, but not presented as absolute values. For A-C, climate means are calculated for seasonal values of each of the three drought types, and for the period covered by the chronology since 1930. The selection of drought years is based on detrended climate data (20-year spline), but SD values are based on the original climate variable.

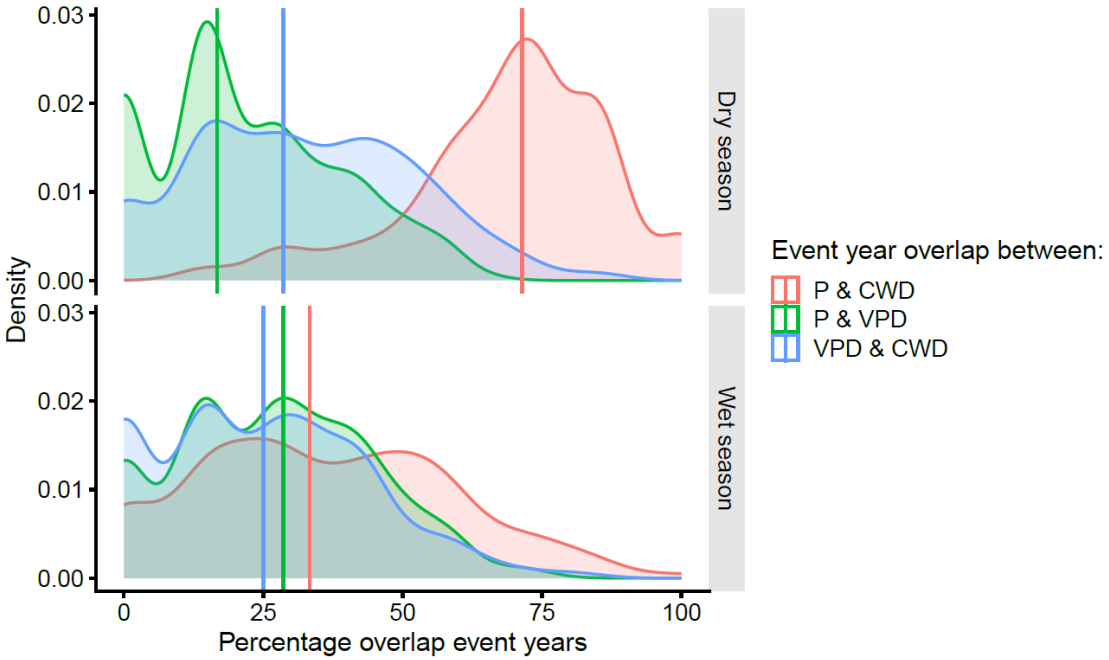

Fig. S5. Overlap of event years between drought types. Distributions of the percentage of identical event years across three drought types (P: precipitation, VPD: Vapor Pressure Deficit, CWD: Climatic Water Deficit), for dry- and wet-season droughts. Vertical lines show median values per comparison. Drought years are identified as the 10% driest years from detrended climate data.

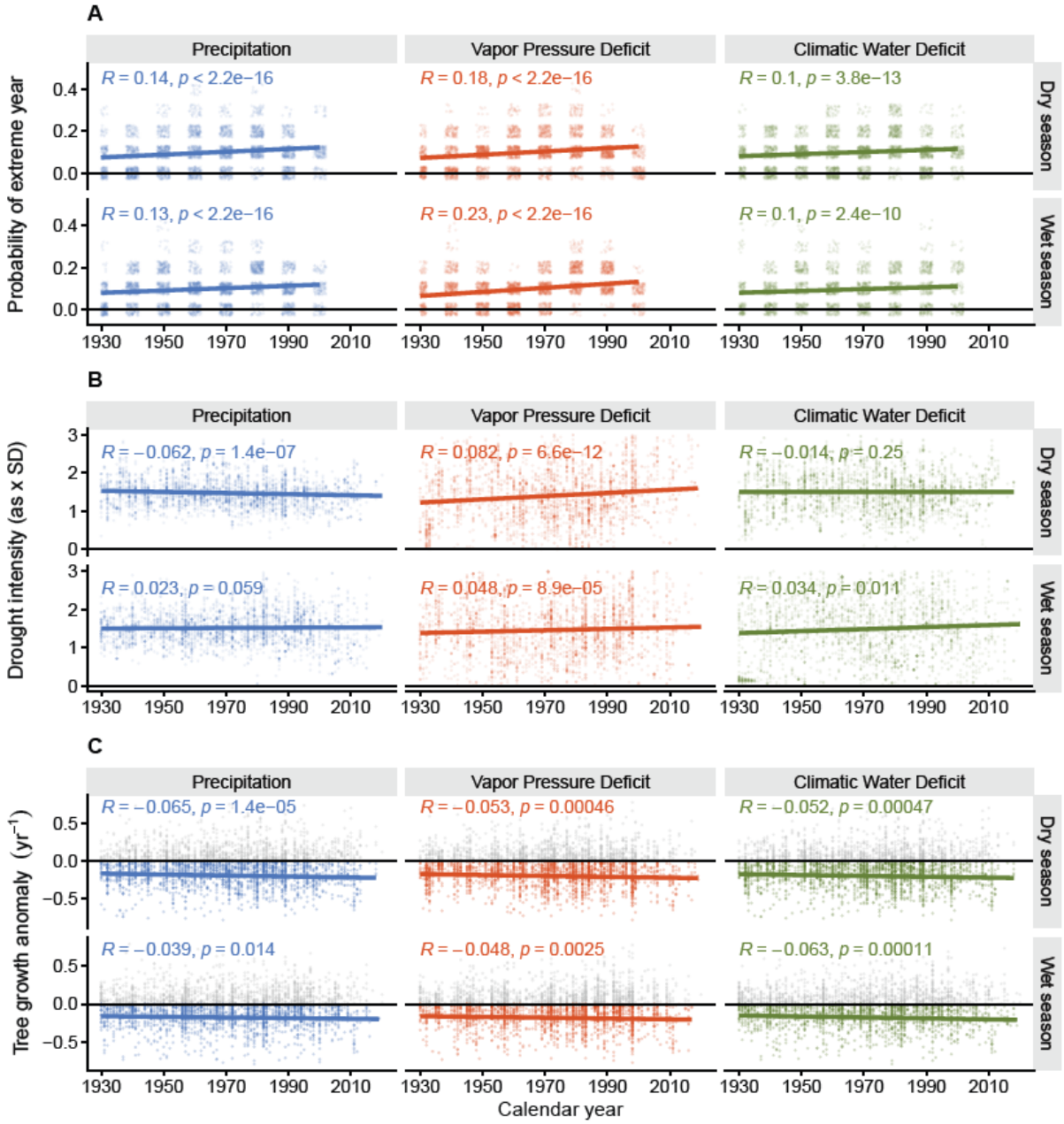

Fig. S6. Shifts in the frequency, intensity and impacts of droughts over time, for three drought types and two seasons. (**A**) Decadal drought probabilities, with each jittered point representing the probability of a drought at one site (chronology) during a (full) decade covered by the chronology. (**B**) Drought intensity for all identified event years, expressed as the number of standard deviations away from the mean. (**C**) Tree growth anomalies during all identified drought years, highlighting negative anomalies (colored). All panels: values are Kendall's Tau correlations coefficients (and p values), testing trends over time (in C for negative anomalies only); lines are for illustration purpose only.

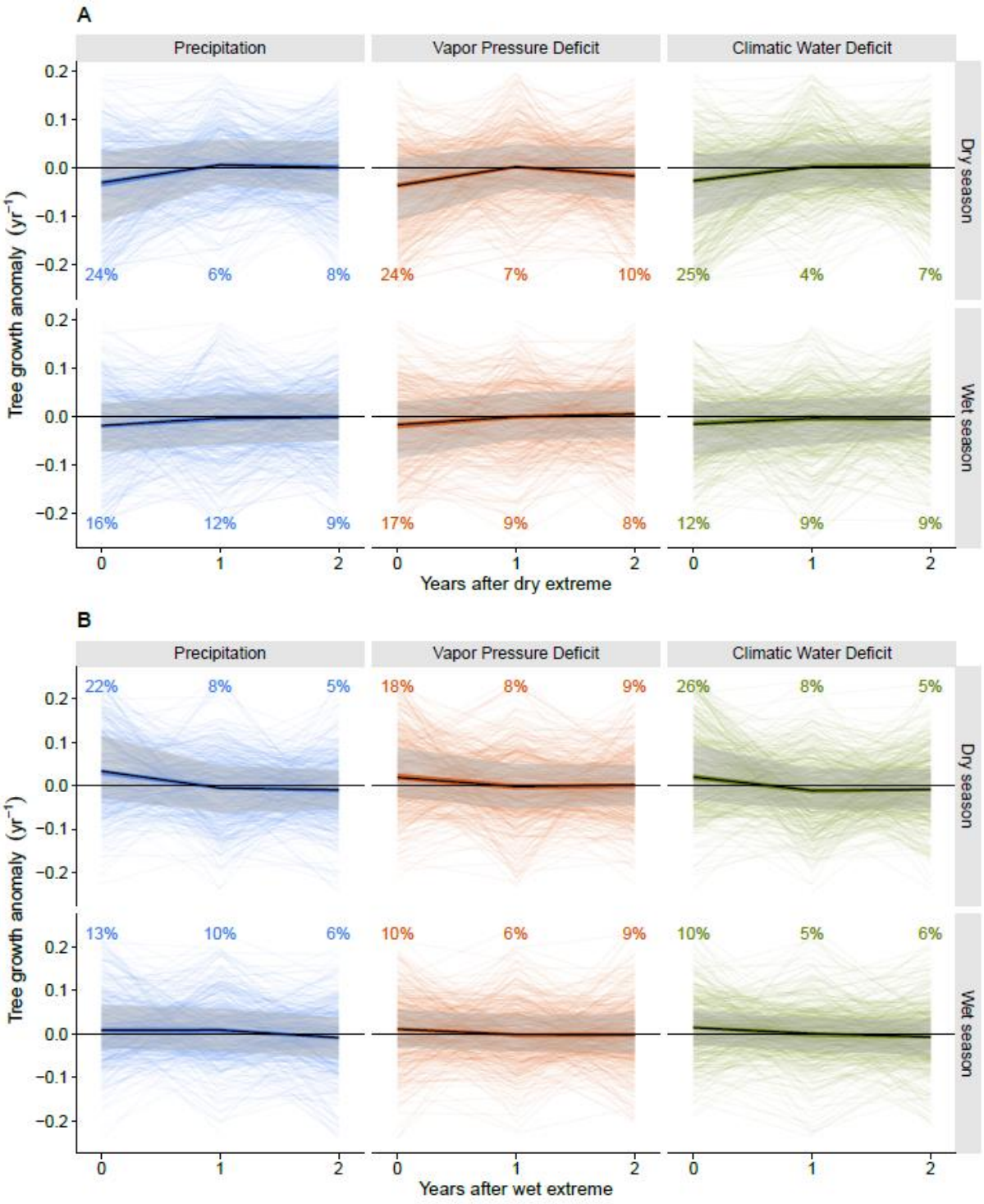

Fig. S7. Responses of tropical trees to the 10% driest (A) and wettest years (B). Thin lines show tree growth anomalies for each of 483 chronologies during and following years with low (A) or high (B) precipitation, high (A) or low (B) vapor pressure deficit or high (A) or low (B) climatic water deficits. Black lines and colored bands represent pantropical medians and their bootstrapped 95% confidence intervals of median responses (n=1000); light grey shaded bands are 25-75% percentiles of the data. Percentage values represent the proportion of significant positive (A) or negative (B) anomalies ($p<0.05$) in SEA analyses.

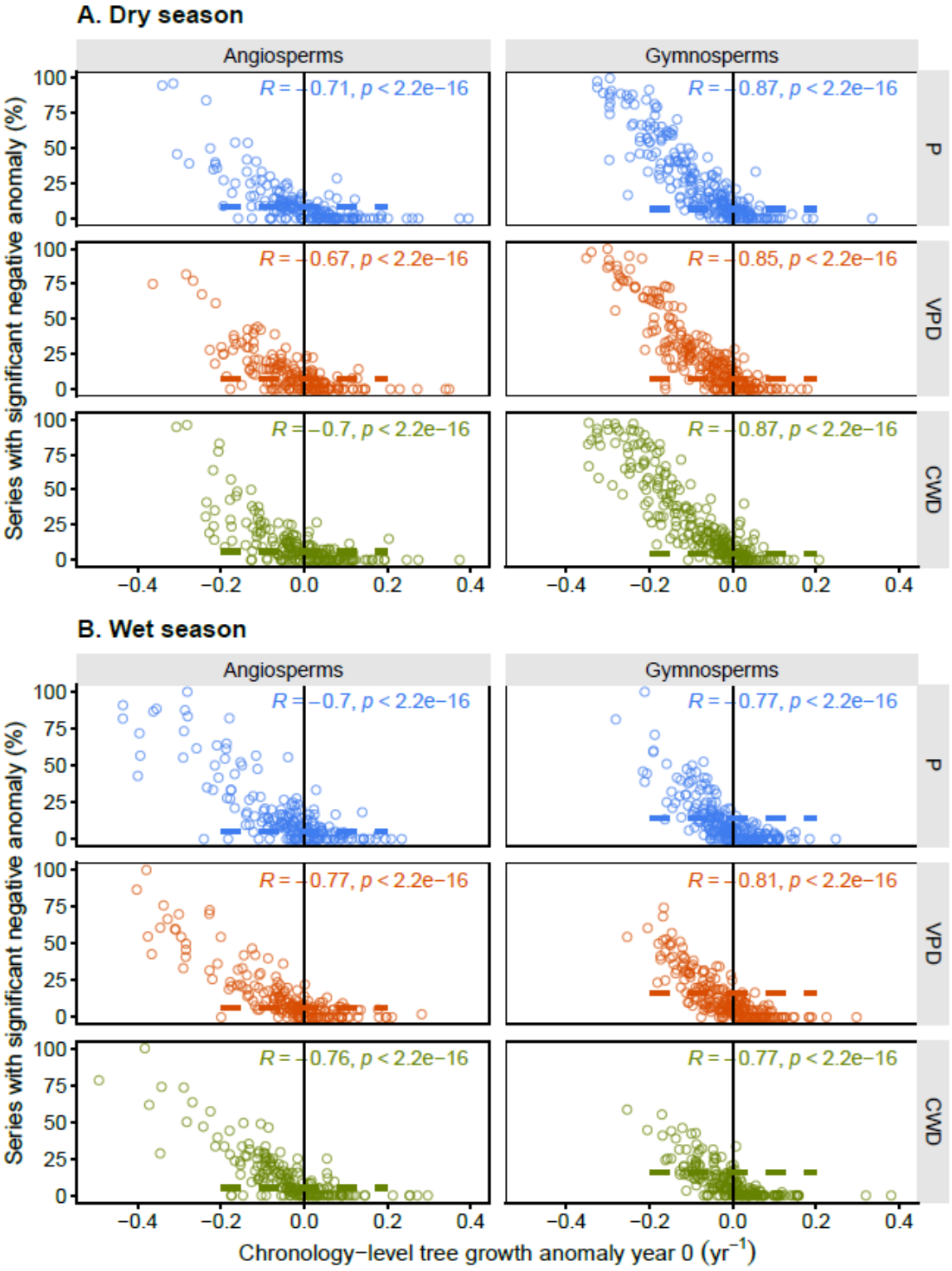

Fig. S8. Association between drought responses at the chronology and series levels. Shown are the drought-induced growth anomalies for each chronology (x-axis) and the percentage of ring-width series exhibiting a significant negative growth anomaly during droughts (y-axis) . Each symbol represents one chronology. Associations between chronology-level anomalies and series-level significance are evaluated for three drought types (P, VPD, CWD), two seasons (A: dry, B: wet) and for angiosperms and gymnosperms separately. Spearman rho and p values are shown. Dashed lines indicate the median percentage of significant series across all chronologies included. Sample sizes: 419-439 chronologies with 14285-15473 series (varies across drought types, seasons and clades).

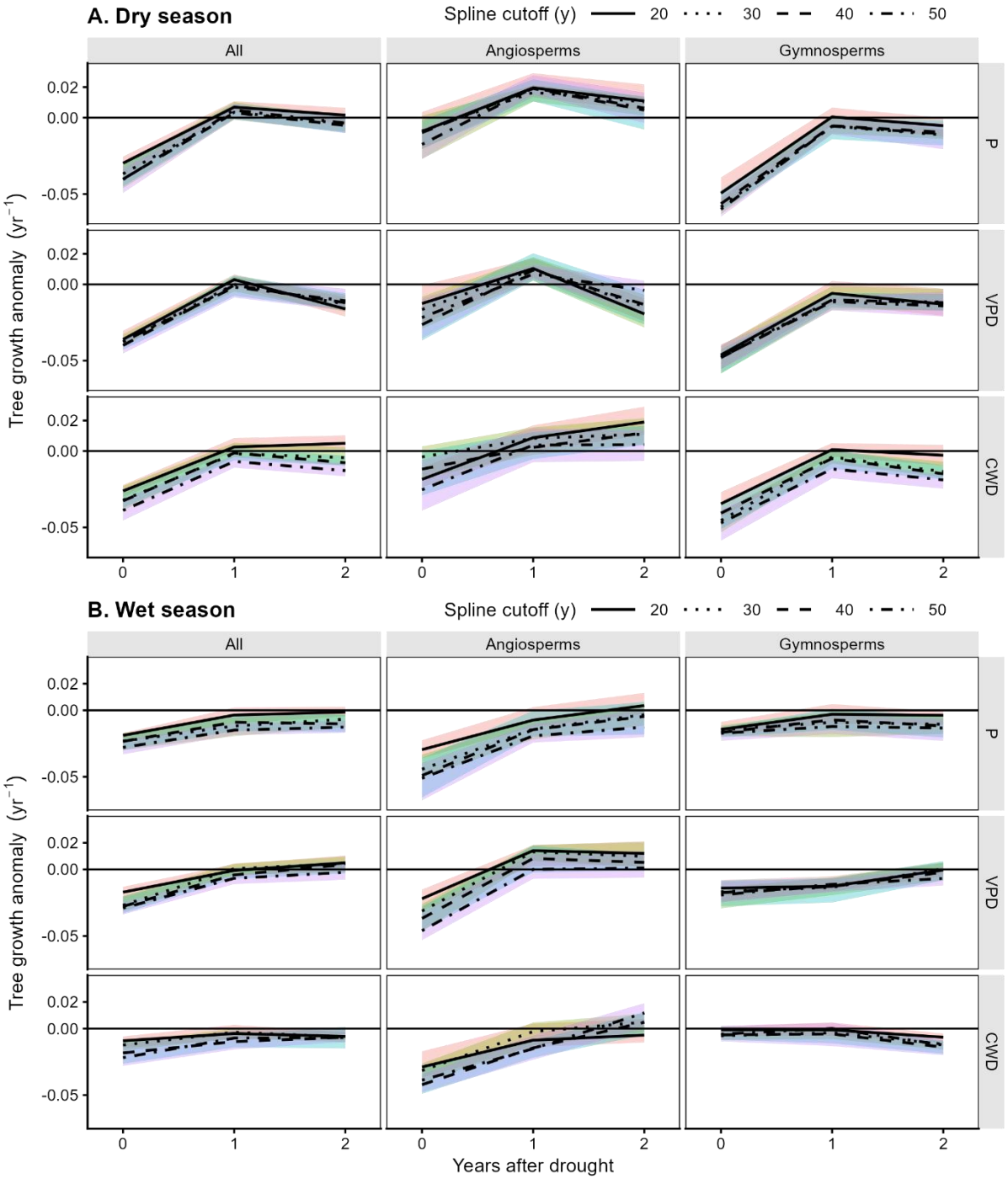

Fig. S9. Robustness of drought responses to more rigid detrending methods. Weighted median tree-growth anomalies (black lines) following years with low precipitation (P), high vapor pressure deficit (VPD) or high climatic water deficits (CWD), for different flexibility of detrending methods and for the dry (A) and wet (B) seasons. Different line types represent results for splines with a 50% frequency cut-off at 20 years (the standard method used, solid) and more rigid versions (30-50 years cut-off). Colored bands are bootstrapped 95% confidence intervals of weighted medians (n=1000). Kruskal Wallis ANOVAs across spline cutoffs were non significant for all combinations of drought types, taxa and seasons, except for dry-season CWD droughts for Gymnosperms (year 1 and 2) and all taxa (year 2).

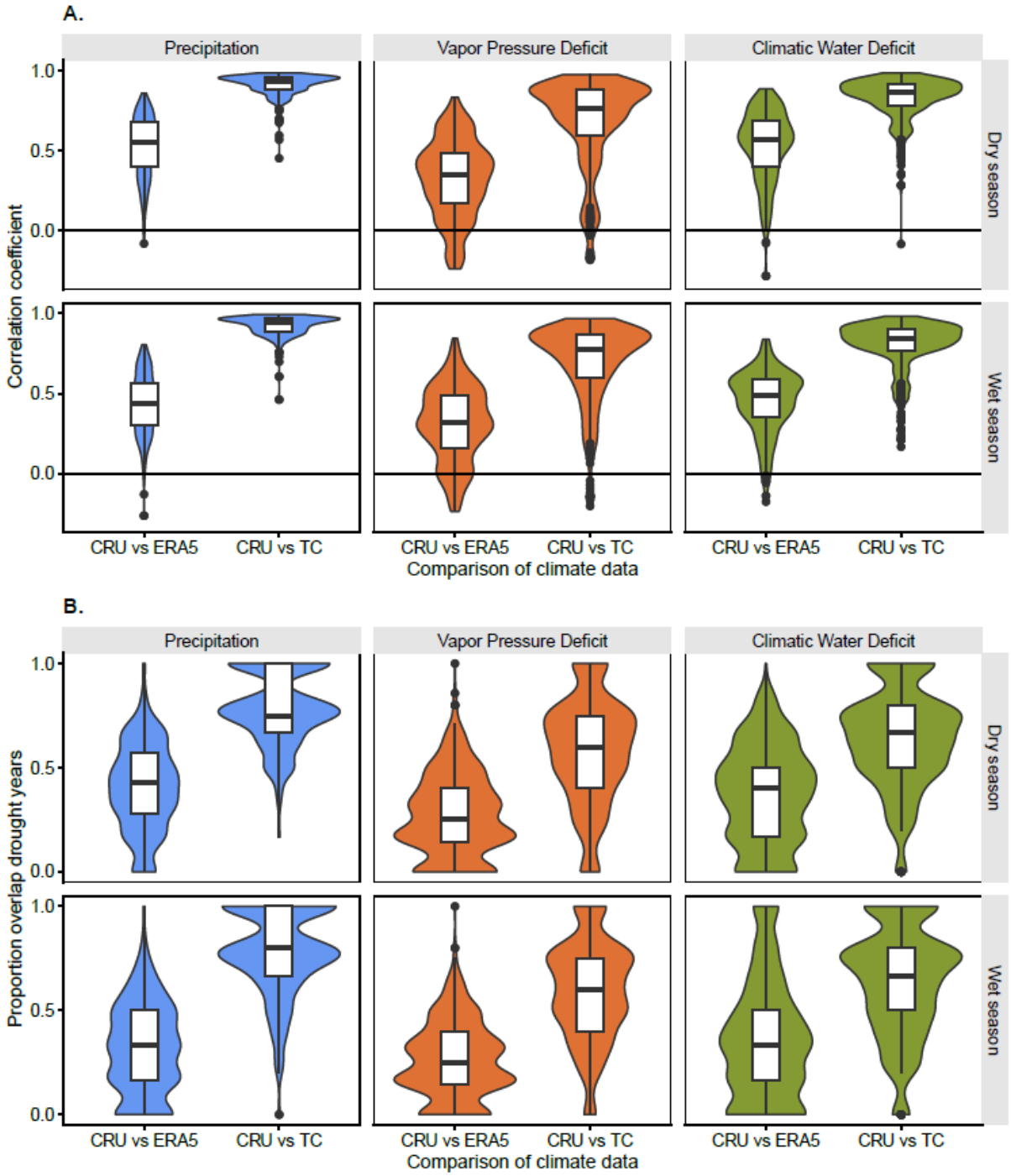

Fig. S10. Climate correlations and detection of drought years for two alternative climate products. (A) Violin plots and boxplots of the Spearman correlations of seasonal climate (P, VPD and CWD) for the common periods of CRU vs ERA5 (1940-2020) and CRU vs TerraClimate (TC, 1958-2020). (B) Proportion of years identified as drought years that overlap when using CRU and ERA5, or CRU and TC. Box hinges correspond to 25th and 75th percentiles, thick middle line is median, whiskers extend to 1.5 times the inter quartile range.

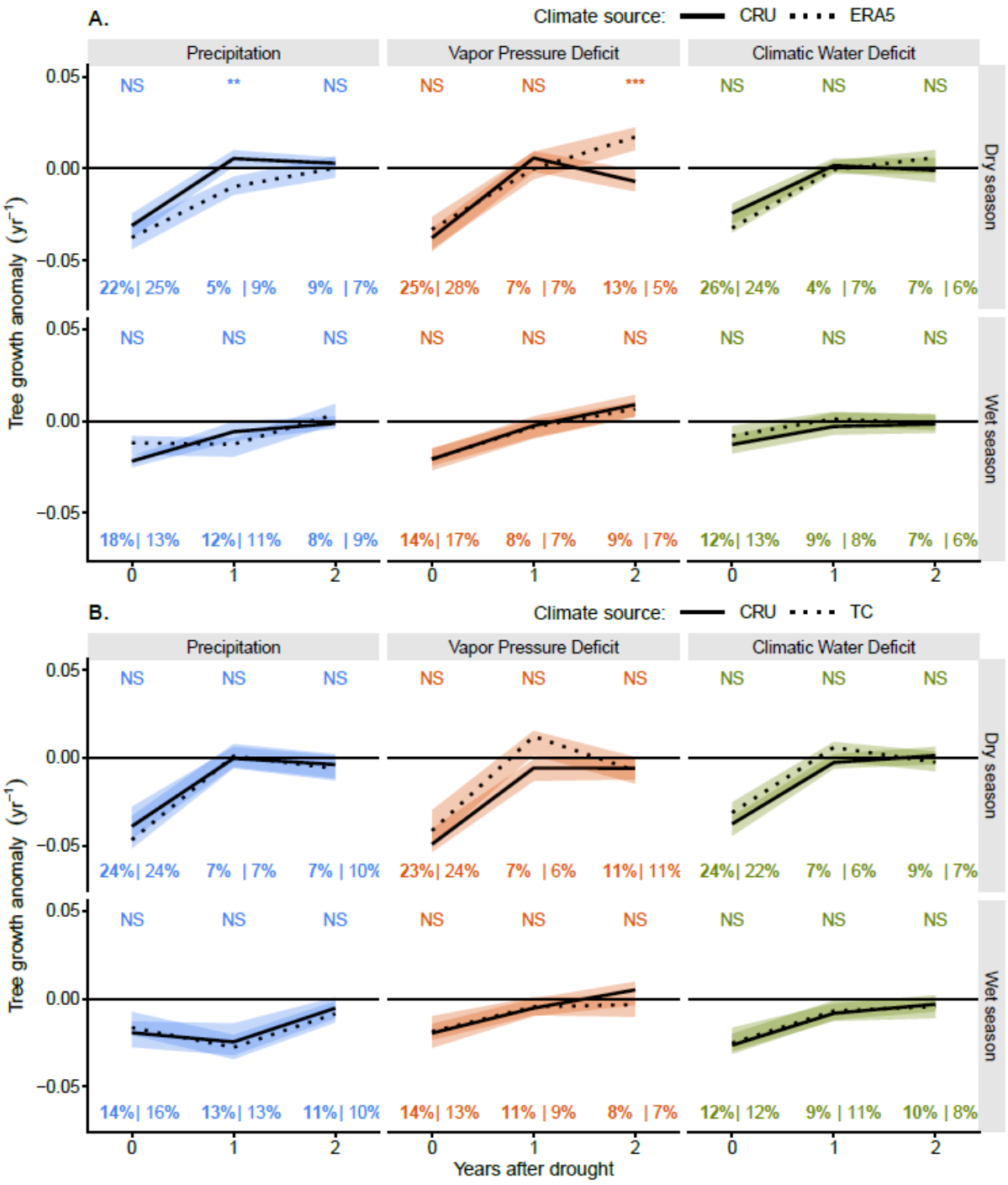

Fig. S11. Robustness of pantropical drought responses to alternative climate sources. Weighted median tree-growth anomalies (black lines) during and following the 10% years with lowest precipitation (P), highest vapor pressure deficit (VPD) or highest climatic water deficits (CWD), for dry and wet season. Growth anomalies are compared between the standard climate product used in the study (CRU, solid lines) and alternative products with higher spatial resolution (dotted lines): (A) TerraClimate (TC, for the overlapping period 1959-2020) and (B) ERA5 (for 1941-2020). Colored bands are bootstrapped 95% confidence intervals of weighted medians (n=1000). Different letters for one year indicate significant differences between climate products (Mann Whitney U tests; $p<0.05$).

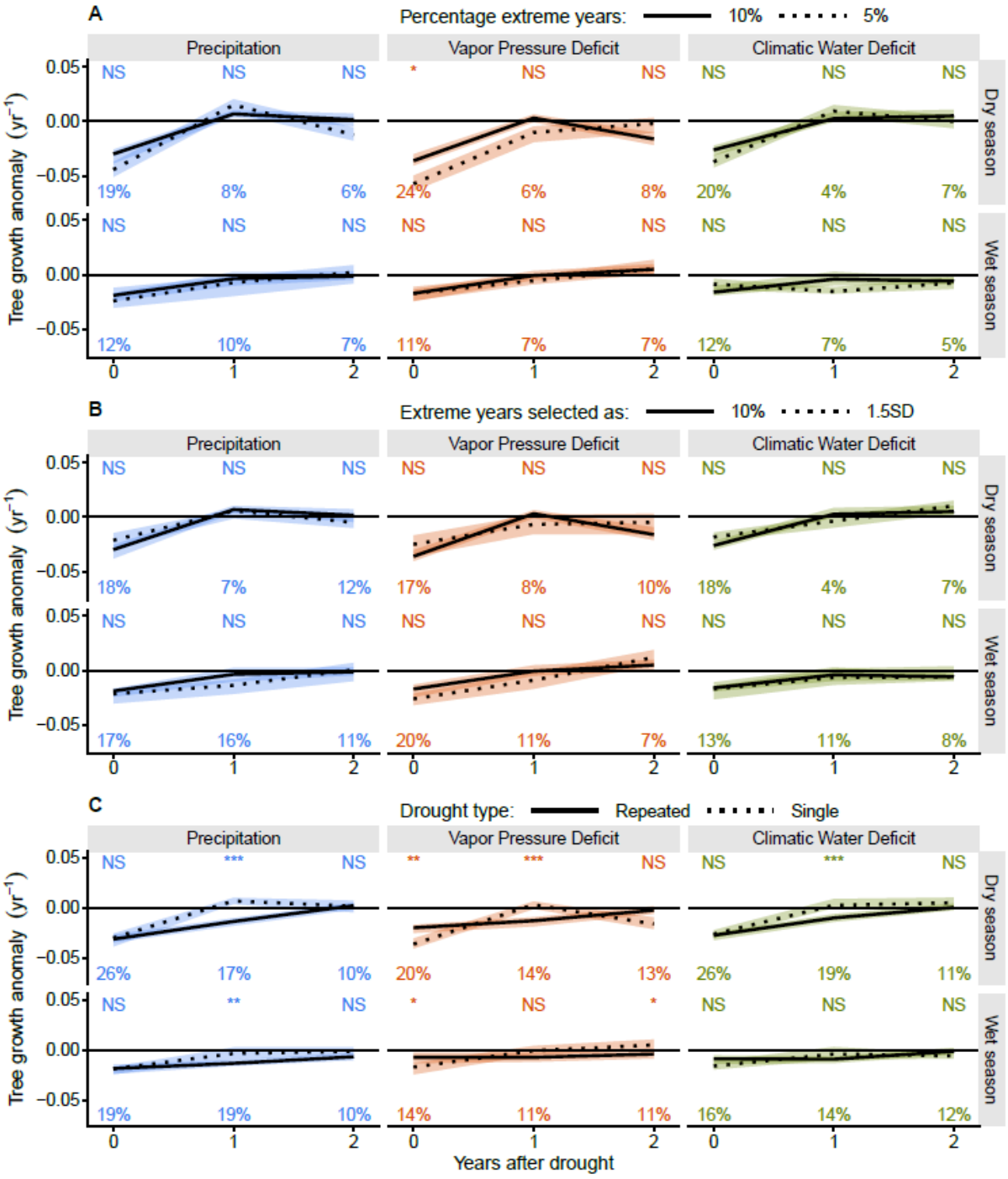

Fig. S12. Sensitivity of pantropical growth anomalies to different ways of selecting extreme years. Comparing the standard extreme year selection (10% of years) with selecting the 5% most extreme years (**A**), years with climatic extremes of >1.5 SD (**B**) or repeated droughts, e.g. 2-year extremes (**C**). In all panels, median tree growth anomalies for standard selection (continuous lines) are compared to an alternative (dotted). Colored bands are bootstrapped 95% confidence intervals of medians (n=1000). Numbers represent percentage of significant ($p<0.05$) negative anomalies for the alternative selection (compare to fig S7A). Results of Mann Whitney U tests between selection methods are shown (NS: non-significant; *: p <0.05; **: p <0.01; ***: p <0.001).

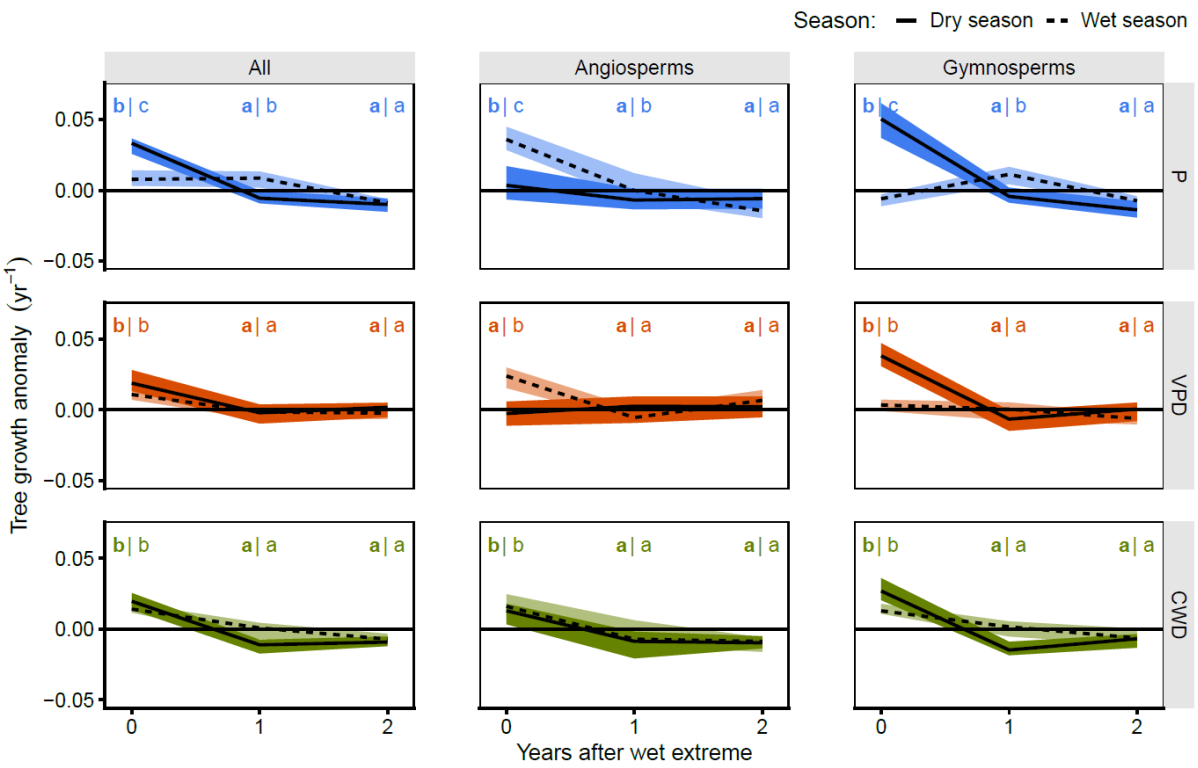

Fig. S13. Pantropical tree growth responses to wet extremes. Growth anomalies during and following years with high precipitation (P), low vapor pressure deficit (VPD), or low climatic water deficits (CWD), for angiosperms and gymnosperms combined and separately. Responses are shown for dry- and wet-season droughts. Bands show bootstrapped 95% confidence intervals of medians (n=1000). Different letters indicate a significant difference between years (Mann Whitney U tests; $p<0.05$) for both seasons (dry in **bold**). Sample sizes: angiosperms 196 sites, gymnosperms 255 sites.

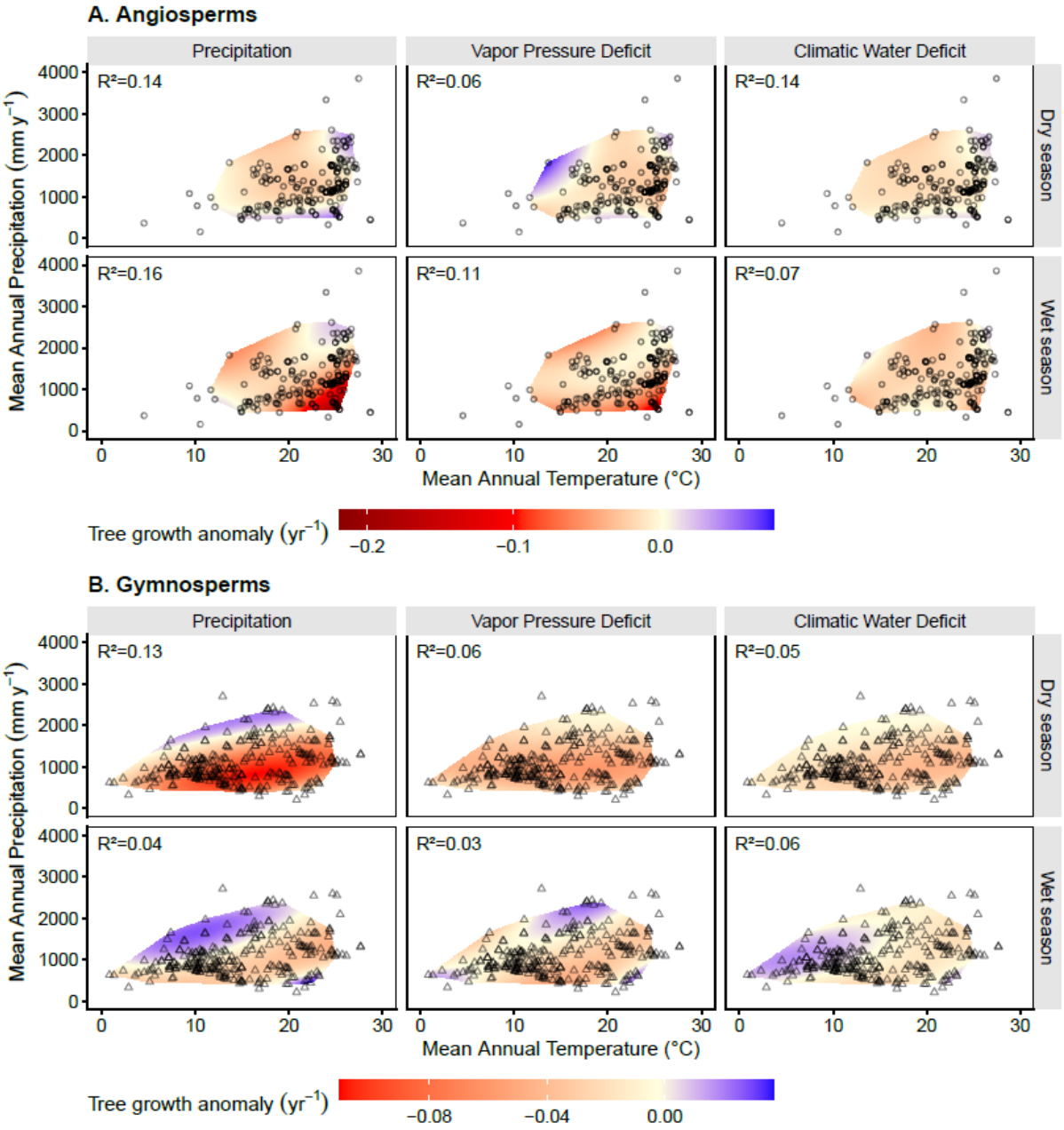

Fig. S14. Drought-induced pantropical growth anomalies interpolated across climate space. Shown are predicted mean growth anomalies for (**A**) angiosperms and (**B**) gymnosperms during years with low precipitation (P), high vapor pressure deficit (VPD) or high climatic water deficits (CWD) for the dry and wet seasons. Symbols indicate site locations.

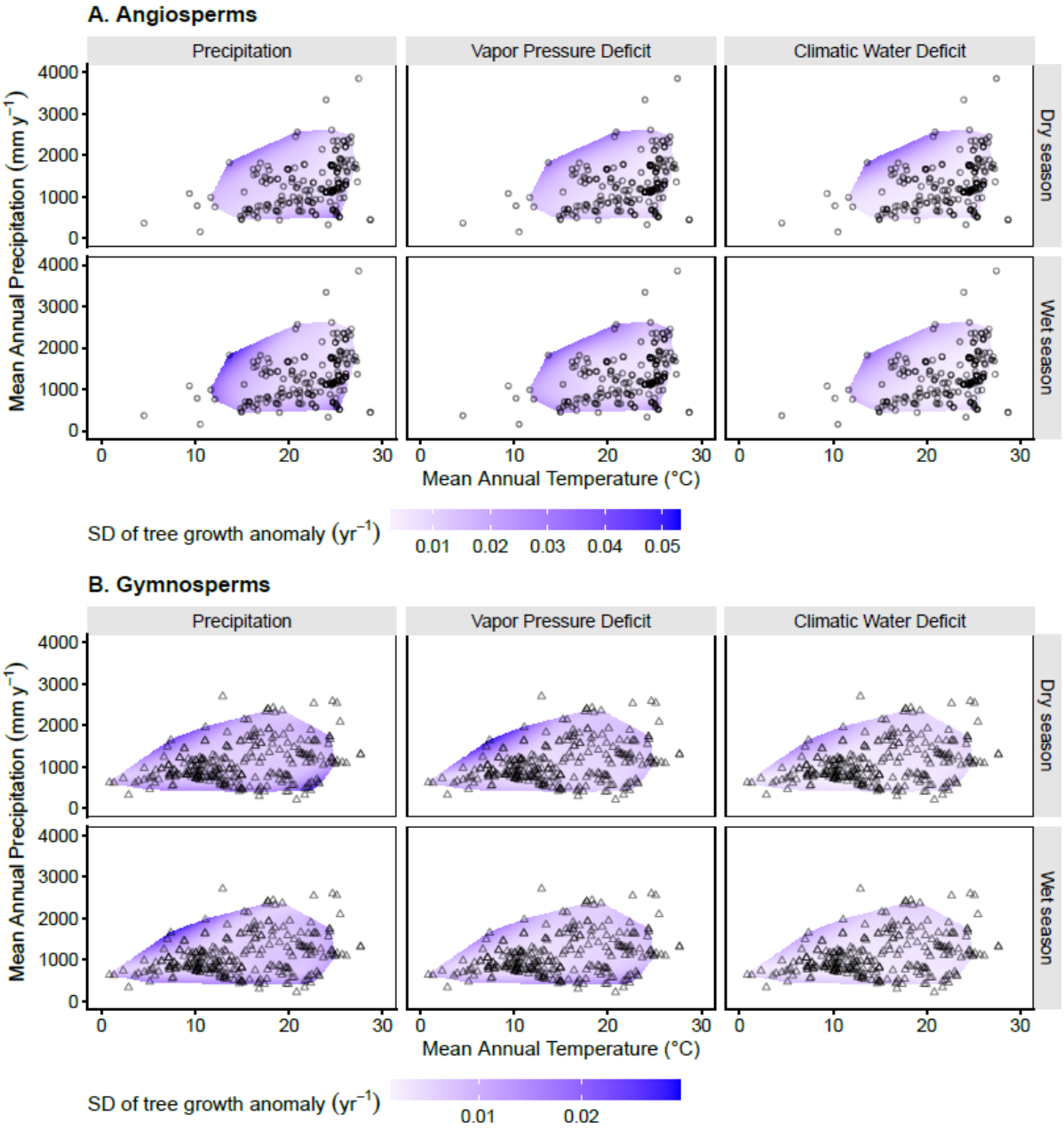

Fig. S15. Uncertainty of interpolation of tropical growth anomalies in response to droughts. As fig S11, but showing the standard deviation of growth anomalies for 1000 random draws (subset 75% of sites).

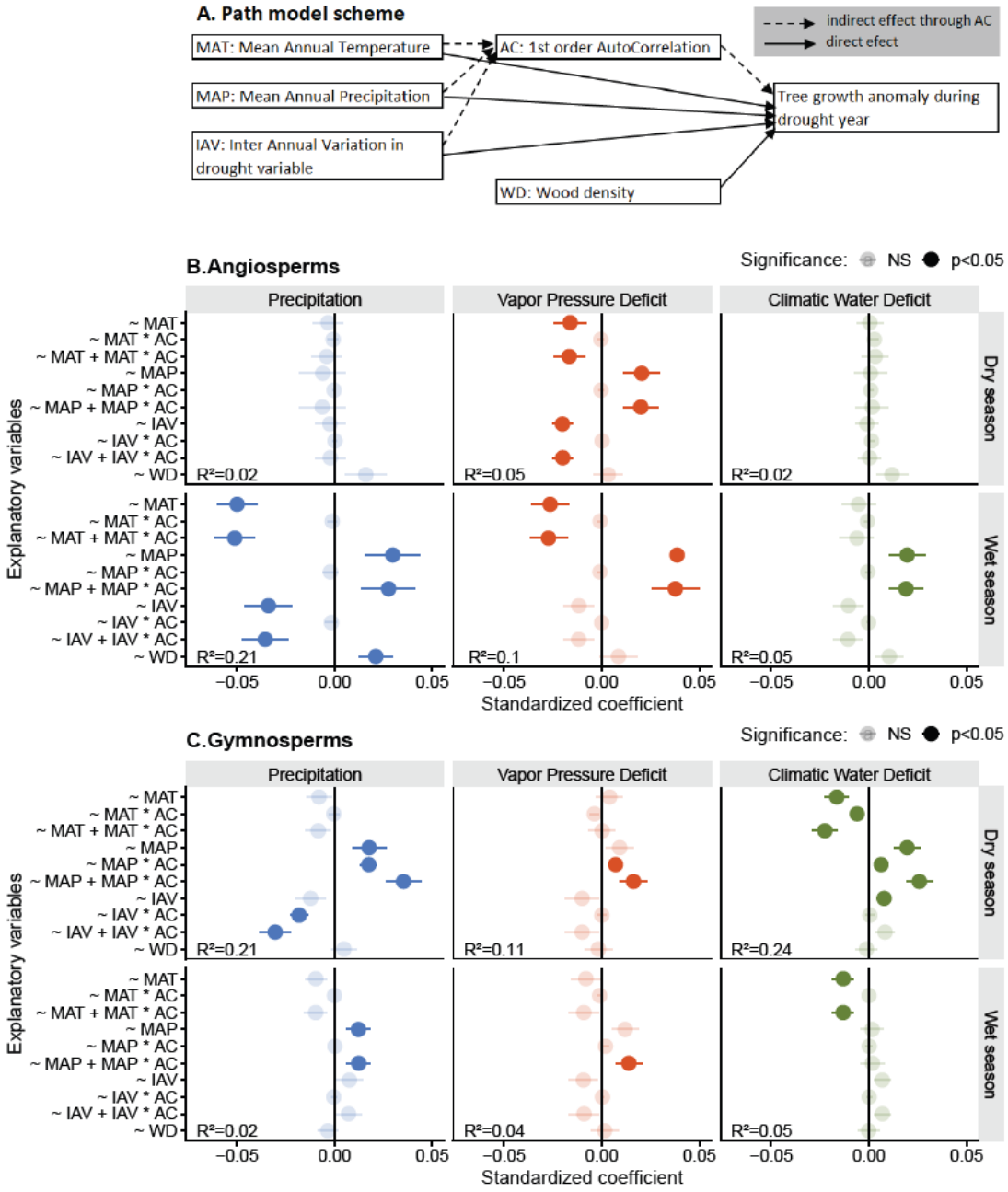

Fig. S16. Direct and indirect drivers of growth anomalies during drought years. (**A**) Path scheme with direct drivers of growth anomalies and indirect drivers resulting from first-order growth autocorrelation (AC). (**B** and **C**) Path analyses results for angiosperms (196 chronologies) and gymnosperms (255 chronologies) for three drought types and two seasons, showing direct effects (~MAT, etc), indirect effects (~MAT*AC, etc), their sums (~MAT + MAP*AC) and wood density (WD) on growth anomalies. Negative values imply that the variable aggravates drought effects.

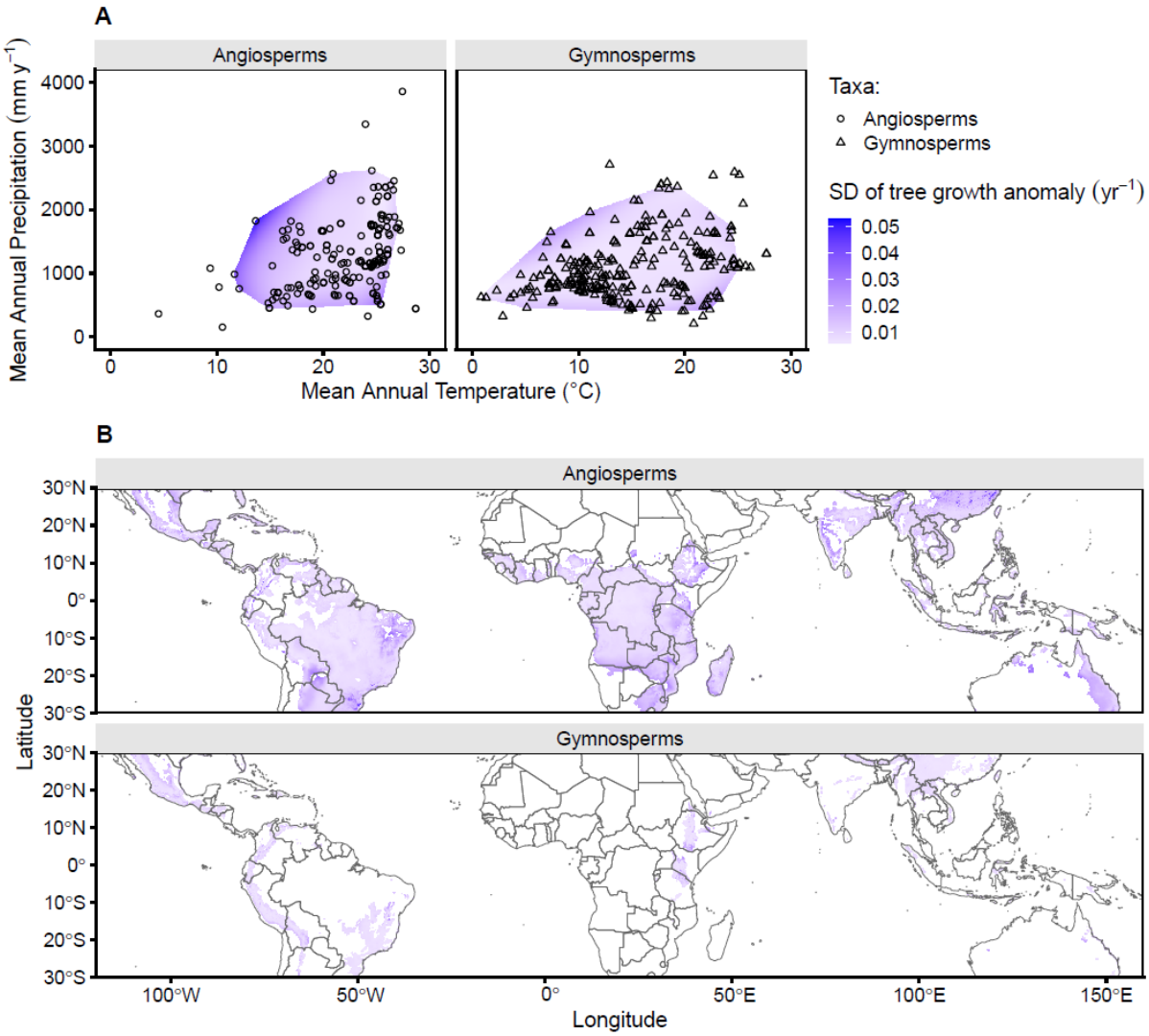

Fig. S17. Uncertainty of interpolated and mapped drought responses of tropical tree growth. (**A**) Standard deviation of growth anomalies during years with low precipitation during the wet (angiosperms, n=210) or dry season (gymnosperms, n=273) interpolated in climate space. The standard deviation of interpolated growth anomalies for 1000 random draws (subset 75% of sites) is presented. (**B**) Geographic projections of the standard deviation of growth anomalies from (A). The geographic distribution of gymnosperms was restricted to elevations >700 m a.s.l. (i.e., the 10th percentile of their elevational distribution) and for Africa in addition by a species distribution model of the only African gymnosperm in our network (*Juniperus procera*).

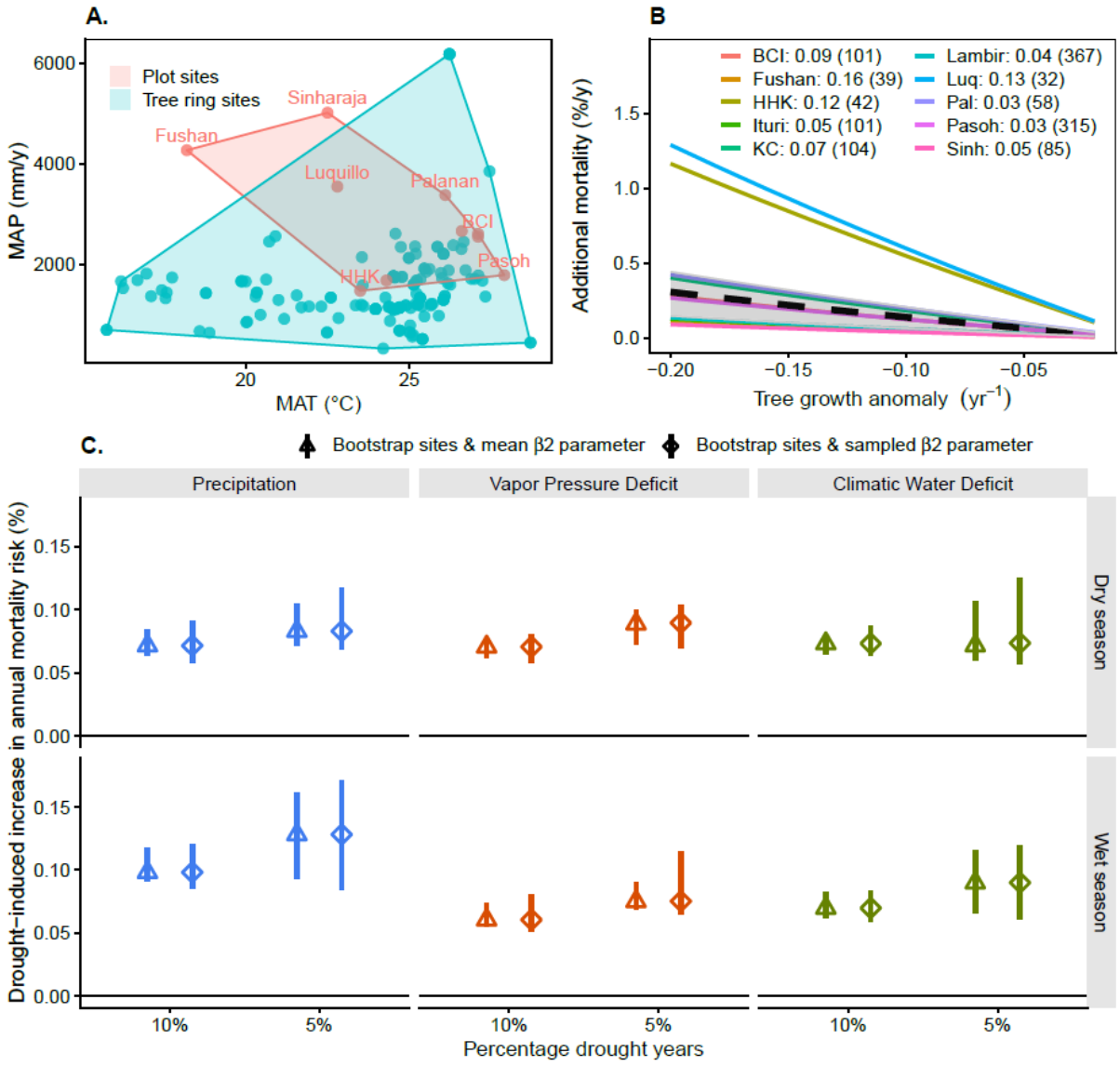

Fig. S18. A first estimate of additional mortality for tropical lowland angiosperms due to drought-induced growth declines. (A) Comparing the climate space of 10 tropical forest monitoring plots (site names included, Ref (*49*)) where growth-mortality associations were quantified, with the 158 lowland angiosperm sites from the tree-ring network. **(B)** Empirical associations between negative growth anomalies and increased mortality from the 10 plots shown in panel A, and the association based on average β2 coefficient (dashed black line), plus or minus 1 SD (grey shaded area). All lines are for trees of at least 20 cm diameter, a standard diameter growth rate of 2 mm per year and against a 1% background mortality (see Methods). Legend shows R^2 values of published associations (and number of species tested) per site. **(C)** Estimated increase in mortality risk due to drought-induced growth reduction for tropical lowland angiosperms. Shown are pantropical median values and their 95% confidence interval for different drought types, seasons, and drought intensities (10% and 5% driest years). Mortality estimations used either the mean coefficient (β2) relating growth anomalies to mortality (dashed black line in panel B) or sampled from the distribution of site-level β2 values. Parameters in the equation were set such that background mortality rate is 1%. Sample sizes: 60-95 chronologies.

Table S1. Median growth anomalies during drought years are similar across drought types, but differ between angiosperms and gymnosperms. (**A**) Results of non-parametric weighted Kruskal-Wallis (across three drought types) for growth anomalies during drought years (year 0) of both seasons and for angiosperms and gymnosperms separately or combined ('All'). (**B**) Results of non-parametric weighted Mann Whitney U tests for growth anomalies during drought years (year 0) between angiosperms and gymnosperms. Both sets of tests relate to the weighted medians shown in Fig. 1B. Sample sizes in terms of number of chronologies are included as 'n'.

A. Across drought types

Clades	Season	Chi squared	p	n
All	Dry season	9.925	0.007	468
All	Wet season	1.727	0.422	449
Angiosperms	Dry season	12.531	0.002	197
Angiosperms	Wet season	6.283	0.043	197
Gymnosperms	Dry season	3.798	0.150	271
Gymnosperms	Wet season	1.572	0.456	252

B. Between clades

Drought type	Season	Chi squared	p	n	n Angio	n Gymno
Precipitation	Dry season	-6.315	<0.001	468	197	271
Precipitation	Wet season	0.373	0.709	449	197	252
Vapor Pressure Deficit	Dry season	-3.104	0.002	468	197	271
Vapor Pressure Deficit	Wet season	-2.371	0.018	449	197	252
Climatic Water Deficit	Dry season	-4.348	<0.001	468	197	271
Climatic Water Deficit	Wet season	1.252	0.211	420	194	226

Data S1. (separate file). Data file (.csv) containing tree growth anomalies during and after (2 years) drought years and wet extremes (10% most extreme years) for all 483 chronologies, and relevant meta-data per chronology. Variables (columns) included: 'Drought_or_wet_extreme' = whether results are for a drought or a wet extreme year; 'SiteID' = ID of chronology; 'Country'; 'Latitude'; 'Longitude'; 'Clade' = whether species is angiosperm or gymnosperm; 'Family'; 'Species'; 'MeanAnnualPrecipitation_mm' = mean annual precipitation in mm (CRU); 'MeanAnnualPrecipitation_degrC' = mean annual temperature in °C (CRU); 'First_year_chronology' = first calendar year of chronology used in analysis (1930 is earliest year); 'Last_year_chronology' = last year of chronology; 'Drought_type' = whether extreme event is in Precipitation, Vapour Pressure Deficit or Climatic Water Deficit; 'Season' = whether an extreme in wet- or dry-season climate is considered; 'Years_after_event' = year after the drought or wet extreme year (thus a value of 0 indicates the event year); 'Growth_anomaly' = anomaly in ring width index (RWI) during event or post-event year, averaged across a minimum of 3 event years; 'Nr_events' = number of events for which growth anomaly is calculated (i.e., 10% of the length of the chronology); 'P_value_SEA' = p-value obtained in SEA analysis, indicating probability that event RWI values are similar to randomly generated RWI values for non-event years; 'Weight' = weight given to growth anomaly when calculating pantropical medians and in statistical analyses, based on density of tropical forested land area for the drought type considered (P, VPD or CWD); 'doi' = Link to raw tree-ring data in the International Tree-ring Databank (ITRDB), hosted by NOAA (https://www.ncei.noaa.gov/products/paleoclimatology/tree-ring); 'NOAAStudyId' = Study ID for the ITRDB.